A TIME-VARIANT PROBABILISTIC MODEL FOR PREDICTING THE LONGER-TERM PERFORMANCE OF GFRP REINFORCING BARS EMBEDDED IN CONCRETE

A Thesis

by

JEONGJOO KIM

Submitted to the Office of Graduate Studies of
Texas A&M University
in partial fulfillment of the requirements for the degree of

MASTER OF SCIENCE

May 2010

Major Subject: Civil Engineering

A TIME-VARIANT PROBABILISTIC MODEL FOR PREDICTING THE LONGER-TERM PERFORMANCE OF GFRP REINFORCING BARS EMBEDDED IN CONCRETE

A Thesis

by

JEONGJOO KIM

Submitted to the Office of Graduate Studies of
Texas A&M University
in partial fulfillment of the requirements for the degree of

MASTER OF SCIENCE

Approved by:

Co-Chairs of Committee,	David Trejo
	Paolo Gardoni
Committee Member,	Daren B.H Cline
Head of Department,	John Niedzwecki

May 2010

Major Subject: Civil Engineering

ABSTRACT

A Time-Variant Probabilistic Model for Predicting

the Longer-Term Performance of GFRP Reinforcing Bars

Embedded in Concrete. (May 2010)

Jeongjoo Kim, B.S., Kyungwon University, Seongnam-si, Gyeonggi-do,

South Korea

Co-Chairs of Advisory Committee: Dr. David Trejo
Dr. Paolo Gardoni

Although Glass Fiber Reinforced Polymer (GFRP) has many potential advantages as reinforcement in concrete structures, the loss in tensile strength of the GFRP reinforcing bar can be significant when exposed to the high alkali environments. Much effort was made to estimate the durability performance of GFRP in concrete; however, it is widely believed the data from accelerated aging tests is not appropriate to predict the longer-term performance of GFRP reinforcing bars. The lack of validated long-term data is the major obstacle for broad application of GFRP reinforcement in civil engineering practices. The main purpose of this study is to evaluate the longer-term deterioration rate of GFRP bars embedded in concrete, and to develop an accurate model that can provide better information to predict the longer-term performance of GFRP bars. In previous studies performed by Trejo et al. (2005), three GFRP bar types (V1, V2, and P type) with two different diameters (16 and 19 mm [0.625, and 0.7 in. referred as #5 and

#6, respectively]) provided by different manufacturers were embedded in concrete beams. After pre-cracking by bending tests, specimens were stored outdoors at the Riverside Campus of Texas A&M University in College Station, Texas. After 7 years of outdoor exposure, the GFRP bars were extracted from the concrete beams and tension tests were performed to estimate the residual tensile strength. Several physical tests were also performed to assess the potential changes in the material. It was found that the tensile capacity of the GFRP bars embedded in concrete decreased; however, no significant changes in modulus of elasticity (MOE) were observed. Using this data and limited data from the literature, a probabilistic capacity model was developed using Bayesian updating. The developed probabilistic capacity model appropriately accounts for statistical uncertainties, considering the influence of the missing variables and remaining error due to the inexact model form. In this study, the reduction in tensile strength of GFRP reinforcement embedded in concrete is a function of the diffusion rate of the resin matrix, bar diameter, and time. The probabilistic model predicts that smaller GFRP bars exhibit faster degradation in the tensile capacity than the larger GFRP bars. For the GFRP bars, the model indicates that the probability that the environmental reduction factor required by The American Concrete Institute (ACI) and the American Association of State Highway Transportation Officials (AASHTO) for the design of concrete structures containing GFRP reinforcement is below the required value is 0.4, 0.25, and 0.2 after 100 years for #3, #5, and #6, respectively. The ACI 440 and AASHTO design strength for smaller bars is likely not safe.

ACKNOWLEDGEMENTS

I would like to thank my committee co-chairs, Dr. Trejo and Dr. Gardoni, and my committee member, Dr. Cline, for their technical guidance and financial support throughout the course of this research.

Thanks also go to my friends and colleagues and the department faculty and staff for making my time at Texas A&M University a great experience. I also want to extend my gratitude to the Texas Department of Transportation (TxDOT) and the Texas Transportation Institute (TTI), which provided funding for this research. I also thank the Zachry Department of Civil Engineering as they provided the test equipment and facilities for this research.

Finally, thanks to my mother and father and to my father-in-law and mother-in-law for their encouragement, and to my wife, Jinhee Seo, for her patience and love.

TABLE OF CONTENTS

Page

Page

LIST OF FIGURES

Page

Page

Page

LIST OF TABLES

Page

1. INTRODUCTION

During the last two decades a significant number of studies have shown that the glass fiber reinforced polymer (GFRP) reinforcing bar may be an economic alternative to conventional steel reinforcement for use in concrete structures. Because corrosion of steel reinforcement can significantly reduce the service-lives of reinforced concrete structures and considering the large rehabilitation cost of existing deteriorating concrete structures, the high corrosion resistance is an attractive benefit of GFRP reinforcement. GFRP reinforcement exhibits high strength to weight ratio and has been reported to be durable.

However, much of the literature indicates that the tensile capacity of the GFRP bar is reduced when exposed to concrete pore solution and moisture. In addition, it is believed that the reduction in strength may be accelerated when sustained loading is applied. In general, when GFRP reinforcement is embedded in concrete, moisture and alkaline solution in the concrete can pass through the protective polymer and attack the glass fiber. This can cause deterioration of the glass fibers and the interfacial area between the glass fibers and the polymer resin, resulting in time dependent reduction in the tensile capacity of the GFRP reinforcing bars. Because the glass fibers account for the majority of the tensile capacity of GFRP bars, the rate at which they deteriorate when embedded in concrete is a critical parameter of estimating reinforcing bar performance

---

This thesis follows the style of *Journal of the American Society of Civil Engineers*.

and eventual overall structural performance.

Due to the time constraints of many research programs, many research projects are carried out using accelerated tests to investigate the environmental factors that primarily affect the longer-term durability of GFRP reinforcement. These results are used to determine the deterioration rate of the GFRP bars when exposed to simulated concrete pore solution. However, debate still remains as to whether exposing GFRP to simulated concrete pore solution is representative of actual field conditions when embedded in concrete. In fact, many researchers believe that simulated exposure condition is excessively harsh and cannot be correlated with the performance of the GFRP bars in actual conditions in field concrete. If this is the case, accelerated testing may not accurately predict the longer-term performance of the GFRP reinforcement embedded in concrete. In addition, in previous research, because the standard experimental methodologies or protocols of the accelerated aging tests have not been well established and test specimens have been placed under various laboratory conditions for various durations, test results are dispersed and sometimes contradictory (Nkurunziza et al. 2005b). The lack of validated and actual longer-term data for durability of GFRP reinforcement as related to civil infrastructure applications makes it difficult for engineers to use this reinforcement (Karbhari et al. 2003). To determine the structural reliability of the GFRP reinforcing bars for reinforcement in concrete structures, civil engineers need longer-term data to justify the use of GFRP reinforcement in structural systems.

The main purpose of this study is to estimate the longer-term deterioration rate of GFRP reinforcing bars embedded in concrete and to construct an accurate predictive capacity model that accounts for influencing parameters.

It is apparent that GFRP bars embedded in concrete beams exposed to actual environments for longer durations can provide more realistic information about the mechanical and physical characteristics of GFRP bars. This data is needed to better predict the longer-term performance of GFRP reinforcing bars and of GFRP reinforced structures. Bayesian updating is used here to develop a probabilistic model for predicting the residual tensile strength of GFRP reinforcement. By using this model, the probability of not meeting the American Concrete Institute (ACI) and AASHTO design strengths considering the environmental reduction factor that represents the detrimental effect of the environment after 100 years is estimated for several diameters of the GFRP reinforcing bars. The probabilistic methodologies offer reliable modeling for predicting the longer-term performance of GFRP reinforcing bars embedded in concrete.

2. RELATED LITERATURE REVIEW

A number of studies have been performed to determine the deterioration rate and to characterize parameters influencing the durability performance of GFRP reinforcement. This literature review describes the accelerated tests and resulting changes in the mechanical properties focusing on the effects of environments such as moisture and simulated pore solution. Then, a review is provided on studies where GFRP reinforcement was embedded in actual concrete environments and residual properties are presented.

2.1. Deterioration of Tensile Capacity in Water or Solutions

As the longer-term durability performance of GFRP reinforcement could depend on properties of the fiber, resin and on the interface between them, the diffusion rate of moisture and alkali through the resin matrix is a critical factor influencing the mechanical deterioration of GFRP bars (Ceroni et al. 2006). When a load is applied to the GFRP, the fibers carry the load and the resin transfers the stress to the fibers. The magnitude of deterioration in the strength of GFRP after exposure to alkaline solutions is strongly related to changes in the stress transfer efficiency between fibers and resin matrix (Abbasi and Hogg, 2005). As most mechanical properties of GFRP are governed by the fibers, if the fibers are not deteriorated, durability can be maintained (Uomoto 2001). The deterioration rate as a function of time for GFRP reinforcing bar is strongly associated with the diffusion characteristic and properties of the resin matrix in GFRP reinforcing bars (Micelli and Nanni 2004).

Nishizaki and Meiarashi (2002) performed deterioration experiments to investigate the longer-term deterioration of GFRP bars submerged in water or moisture. The authors reported that GFRP specimens immersed in water at $60^{o}C$ $(140^{o}F)$ for 434 days present faster separation between the glass fibers and the resin matrix than specimens exposed to partially saturated conditions. The authors also indicated that the water and moisture levels are clearly factors contributing to the longer-term deterioration of GFRP bars.

Katsuki and Uomoto (1995) studied the alkali penetration into the glass fibers of GFRP reinforcement with vinylester resin. In their study, specimens were immersed in 1.0 mol/l aqueous NaOH solutions at $40^{o}C\,(104^{o}F)$ to accelerate the deterioration. It was recorded that loss in the tensile strength was up to 60 percent after 120 days of exposure to alkaline solution. To protect the glass from alkali attack, the authors recommended that the thickness of the layer of the resin be controlled.

Tannous and Saadatmanesh (1998), Sen et al. (2002), Micelli and Nanni (2004), Chu et al. (2004), Trejo et al. (2005), Nkurunziza et al. (2005a), Chen et al. (2005), and Kim et al. (2007) performed accelerated aging tests by conditioning with water and alkaline solutions to investigate changes in mechanical properties and moisture uptake of GFRP reinforcement. Based on the accelerated tests, test results showed that the alkaline solution is more detrimental to the durability of GFRP than water (Chu et al. 2004).

In addition, the GFRP with polyester resin has been reported to exhibit inferior durability performance as compared to GFRP with vinylester resin (Tannous and Saadatmanesh 1998).

Tannous and Saadatmanesh (1998) investigated changes in moisture contents and mechanical properties of GFRP reinforcing bars when saturated in different chemical solutions. GFRP reinforcing bars of different diameters (10 and 20 mm, 0.4 and 0.8 inch, respectively) made of polyester and vinylester resins were immersed in different solutions. The selected environments were water at 25 ^{o}C (77 ^{o}F) and saturated $Ca(OH)_2$ solutions with pH values of 12 exposed to temperatures of 25 ^{o}C and 60 ^{o}C (140 ^{o}F). An acidic solution with a pH of 3 was used to simulate infiltration of acidic chemicals through cracked concrete. In addition, the solutions of 7 percent weight of NaCl+$CaCl_2$ (2:1 weight mixtures) and the solutions of 7 percent weight of NaCl+$MgCl_2$ (2:1 weight mixtures), simulating seawater, were used in this study.

After 6-months of immersion in each environment, the moisture contents and residual tensile strengths of the specimens were estimated. In General, higher losses in the strength were observed for specimens in the alkaline solution and deicing salt solution than for the specimens immersed in water. For 10 mm (0.4 inch) diameter bars made of polyester resin immersed in the alkaline solution at temperatures of 25 ^{o}C (77 ^{o}F) and 60 ^{o}C (140 ^{o}F) the measured losses in the strength were 25 and 28.6 percent, respectively. For the same diameter bars made of vinylester resin the measured losses were 13 and 20.3 percent, respectively. Based on these test results, it was

determined that the diffusion rate increases with temperature and vinylester resin presents lower diffusivity rate absorption rates and exhibits higher resistance to alkali attack than GFRP bars with polyester resin.

Accelerated aging tests with alkali-resistant (AR) glass fibers using the same test methodologies were performed by Tannous and Saadatmanesh (1999). This study focused on assessing the changes in mechanical properties of the GFRP bars made with the AR glass fibers. In terms of the tensile response, the AR glass did not improve the durability of GFRP reinforcement in the alkaline environment, and it is believed that the quality control during pultrusion makes a difference in the quality and the durability of GFRP bars. The authors also indicated that although Fick's law can be applied to relatively short-term prediction in accelerated aging tests, it will not be applied for prediction of the longer-term performance of GFRP bars due to the micro-cracking and progressive matrix damages.

Micelli and Nanni (2004) performed accelerated aging tests to investigate the residual properties of GFRP bars made of thermoplastic and polyester resin. Specimens fabricated with E-glass fibers and thermoplastic and polyester resins were exposed to simulated pore solution with an average pH of 12.6 at $60^{\circ}C\,(140^{\circ}F)$. The measured losses in tensile strength of GFRP bars containing polyester resin after 21 and 42 days exposure to alkaline solution were 30 and 40 percent of the ultimate strength. No significant deterioration was reported in the GFRP bars made with thermoplastic resins and immersed in alkaline solution. The authors concluded that the resin properties have

an important influence on the durability of GFRP reinforcement, and polyester resin does not provide sufficient protection from alkali attack and reductions in strength.

Chu et al. (2004), Chen et al. (2005), and Kim et al. (2007) performed accelerated aging tests with similar methodologies and conditioning for the short-term durability performance of GFRP reinforcement. GFRP reinforcement made of E-glass and vinylester resin was exposed to moisture, chloride, and alkalis for specific durations.

Chu et al. (2004) investigated the deterioration rate and the degradation mechanism of GFRP reinforcement exposed to different temperatures. Specimens were exposed to de-ionized water and simulated concrete pore solution (pH of 11.5) at $23^{o}C\,(73.4^{o}F)$, $40^{o}C\,(104^{o}F)$, $60^{o}C\,(140^{o}F)$, and $80^{o}C\,(176^{o}F)$. In this study, the deterioration was accelerated using elevated temperatures then results were characterized through tension tests and moisture uptake measurements. The rate of moisture uptake was reported to increase with temperature. Specimens immersed in alkaline solutions at the highest temperature exhibited maximum moisture uptake and the highest diffusion rates. The authors reported that this is primarily due to the hydrolysis and plasticization of the resin matrix due to the penetration of the high pH solution, which induced micro-cracking of the resin. The reduction in tensile capacity for specimens immersed in alkaline solution was more severe than the specimens immersed in water. The residual tensile strength of specimens in alkaline solution was 86.3, 68.8, 55.9, and 46.3 percent, as compared to 92.4, 70.9, 58.8, and 48 percent when immersed in water at $23^{o}C\,(73.4^{o}F)$, $40^{o}C\,(104^{o}F)$, $60^{o}C\,(140^{o}F)$, and $80^{o}C\,(176^{o}F)$, respectively.

Chen et al. (2005) performed accelerated aging tests using elevated temperatures and five different pore solutions to simulate exposure of specimens to actual field conditions. The selected five solutions were: 1) tap water; 2) simulated pore solution of normal concrete (NC) with pH of 13.6; 3) simulated pore solution of high performance concrete (HPC) with pH of 12.7; 4) mixtures of sodium chloride and sodium sulfate simulating ocean water; and 5) mixtures of sodium chloride and potassium hydroxide (pH of 13) which simulated concrete pore solution contaminated with deicing salts. All specimens were immersed in solutions for 70 days at $60\,^{o}\mathrm{C}\,(140\,^{o}\mathrm{F})$. The residual tensile capacities of the GFRP bars in solutions 1, 2, 3, 4, and 5 were measured to be 70, 64, 73, 74, and 52 percent, respectively.

Trejo et al. (2005) investigated changes in physical properties of GFRP reinforcement in water and alkaline solutions at different temperatures. GFRP reinforcing bars with diameters of 16 and 19 mm (0.63 and 0.75 inch, respectively) provided by three different manufacturers were assessed (V1, V2, and P). Schaefer (2002) indicated that the V1 and V2 were made of E-glass and vinylester and P type bar was made of E-glass and polyethylene terephthalate (PET) polyester matrix. All specimens were immersed in water and simulated pore solution with pH of 12 for up to 350 days. The losses in the tensile strength for the V1, V2, and P type bars after 350 days conditioning at $35\,^{o}\mathrm{C}\,(95\,^{o}\mathrm{F})$ were 7.28, 12.31, and 15.81 percent when immersed in water and 8.87, 15.21, and 13 percent when immersed in high pH solution, respectively. Based on short-term data, a time dependent model was updated with a

reduction factor, taking into account tensile properties associated with the diffusion rate. However, an accurate value of the reduction factor was not determined.

Sen et al. (2002), Nkurunziza et al. (2005a), and Debaiky et al. (2006) investigated the durability performance of GFRP reinforcement in different environments combined with a range of sustained stresses. Sen et al. (2002) indicated that because two penetration mechanisms of solution in concrete are resin cracking under load and diffusion through the resin matrix, data on the performance of GFRP bars subjected to high alkaline environments at various stress levels is useful for the evaluation of structures containing GFRP reinforcement. For the case of GFRP bars in moist concrete under sustained loads, three types of stress corrosion mechanism were identified by Benmokrane et al. (2002). These were reported to be stress dominated, crack propagation dominated, and diffusion dominated. It was reported that the applied stresses on the GFRP bars at high temperatures can form cracks in the resin which accelerates the penetration of alkalis through the resin into the glass fibers.

The main objective of this study performed by Sen et al. (2002) is to evaluate the effects of sustained stress on the diffusion rate and reduction in the tensile strength of GFRP reinforcement. Specimens were exposed to simulated concrete pore solution with a pH of 13.5 under constant loads 10 and 25 percent of the ultimate tensile strength. Control specimens were unloaded. Tension tests were conducted to determine the residual strength after exposure for 1, 3, 6, and 9 months. After 9 months exposure, losses in the tensile strength were reported to be 63 and 70 percent at the 0 and 10 percent stress levels, respectively. In the case of the 25 stress level, the failure of the

GFRP reinforcing bar occurred within 25 days of starting the test. Based on the significant difference in durability between the stressed and unstressed specimens, Sen et al. (2002) concluded that resin cracking by the sustained stress plays an important role in the degradation process, especially, at higher stress levels.

Nkurunziza et al. (2005a) also investigated the residual tensile capacity of GFRP bars subjected to simulated concrete pore solution under sustained loading. Specimens were exposed to de-ionized water and alkaline solution and subjected to two kinds of sustained axial loading, 25 and 38 percent of the ultimate strength. The residual tensile strength was measured after exposure. The authors concluded that the reduction in tensile capacity was influenced more by the effects of water absorption than by the effects of the alkalinity at lower stress. As the widths of the micro-cracks in the resin increased with stress level, it was easier for smaller water molecules to permeate into the glass fibers through the resin matrix. However, when the micro-cracks become large enough to allow alkaline molecules to pass at high stress level, the damage by alkalis exceeds that of water and the failure is dominated by propagation of micro-cracks.

Debaiky et al. (2006) evaluated the residual tensile capacity of three sizes of GFRP reinforcing bars at elevated temperatures in alkaline solution (pH=12.7) and water (pH=7) environments combined with sustained loading. Bar diameters of 16 mm (0.63 inch), 12.7 mm (0.5 inch), and 9.5 mm (0.37 inch) were loaded from 18 to 29 percent of the guaranteed tensile strength for 1 to 4 months and then tested for residual tensile capacities. The 16 mm (0.625 inch) diameter GFRP bars showed 10 and 15.9 percent capacity losses in water and alkaline solution after 2 months of immersion, respectively.

The reduction in tensile capacity of the 12.7 mm (0.5 inch) diameter bars conditioned for 4 months were 15.5 and 17.2 percent when immersed in water and alkaline solutions, respectively. For the 9.5 mm (0.37 inch) diameter bars conditioned for 2 months, measured losses of tensile capacity were 1.66 for water and 9.94 percent for the alkaline solution. It was reported that small bars shows a slight increase in elastic modulus after conditioning due to more curing of the matrix at high temperature. In the micro-structural analysis, the de-bonding mechanism, which is reported to weaken the interface of the glass and the resin, and hydrolysis of the resin were observed. However, degradation of the glass fibers was not detected.

Table 1 and 2 provide the summary of the loss in tensile capacity of GFRP bars obtained from accelerated aging tests immersed in water and simulated pore solutions reported in the literature.

Table 1. Summary of the deterioration of GFRP (polyester) in water or solutions

Bar Types (matrix /glass)	Bar Diameter mm. (inch)	Conditioning (immersion in)	Exposure Temp. ^{o}C (^{o}F)	Exposure Duration (days)	Applied Stress (%)	Capacity Loss (%)	Reference
Polyester /E-glass	6.35 (0.25)	alkaline solution (pH=12.6)	60 (140)	21	0	30.39	Micelli and Nanni, 2004
				42		40.61	
Polyester /E-glass	10 (0.39)	water	25 (77)	180	0	6.27	Tannous and Saadatmanesh, 1998
		alkaline solution pH=12	60 (140)			28.58	
Polyester / AR-glass	10 (0.39)	water	25 (77)	180	0	7.34	Tannous and Saadatmanesh, 1999
		alkaline solution pH=12	60 (140)			28.00	
Polyester /AR-glass	9.3 (0.37)	alkaline solution (aqueous NaOH)	40 (104)	140	30	4.89	Benmokrane et al. 2002
Polyester / E-glass (P)	15.88 (0.625)	distilled water (pH=7)	35 (95)	350	0	15.81	Trejo et al. 2005
		alkaline solution (pH=12)	35 (95)	350		13	

Table 2. Summary of the deterioration of GFRP (vinylester) in water or solutions

Bar Types (matrix /glass)	Bar Diameter mm. (inch)	Conditioning (immersion in)	Exposure Temp. ^{o}C (^{o}F)	Exposure Duration (days)	Applied Stress (%)	Capacity Loss (%)	Reference
Vinylester /E-glass	12.7 (0.5)	water	80 (176)	132	0	21.9	Kim et al. 2007
		alkaline solution (pH=13)	80 (176)	60		39.7	
Vinylester /E-glass		water	80 (176)	70	0	52	Chu et al. 2004
		alkaline solution (pH=11.5)	80 (176)	70		53.7	
Vinylester /E-glass	9.53 (0.38)	water	60 (140)	70	0	29.44	Chen et al. 2005
		solution (pH=13.6)/ simulate NC		70		36.06	
Vinylester /E-glass	9.5 (0.37)	de-ionized water (pH=7)		417	25	7.29	Gilbert Nkurunziza et al. 2005a
		alkaline solution (pH=12.8)		417	38	34.88	
Vinylester /E-glass	12.7 (0.5)	water (pH=7)	60 (140)	120	25.8	15.5	Debaiky et al. 2006
		alkaline solution (pH=12.8)	54 (129)	120	24.4	17.2	
	9.5 (0.37)	water (pH=7)	72 (162)	60	0	1.66	
		alkaline solution (pH=12.8)	65 (149)	60	0	9.94	
Vinylester /E-glass	10 (0.39)	water	25 (77)	180	0	2.89	Tannous and Saadatmanesh 1998
		alkaline solution (pH=12)	60 (140)			20.29	
Vinylester /AR-glass	10 (0.39)	water	25 (77)	180	0	5.86	Tannous and Saadatmanesh 1999
		alkaline solution (pH=12)	60 (140)			22.66	
Vinylester /E-glass	9.5 (0.37)	kept open in water tank	60 (140)	270	0	57.71	Mukherjee and Arwikar 2005
Vinylester /E-glass	8 (0.31)	pH=13.55		270	0	63	Sen et al. 2002
				270	10	70	
				25	25	100	
Vinylester / E-glass (V1)	15.88 (0.625)	water (pH=7)	35 (95)	350	0	7.28	Trejo et al. 2005
		alkaline solution (pH=12)		350		8.87	
Vinylester / E-glass (V2)	15.88 (0.625)	water (pH=7)		350	0	12.31	
		alkaline solution (pH=12)		350		15.18	

The normalized residual tensile capacities for GFRP bars immersed in water and simulated pore solutions are plotted against exposure time in Figs.1 through 2.

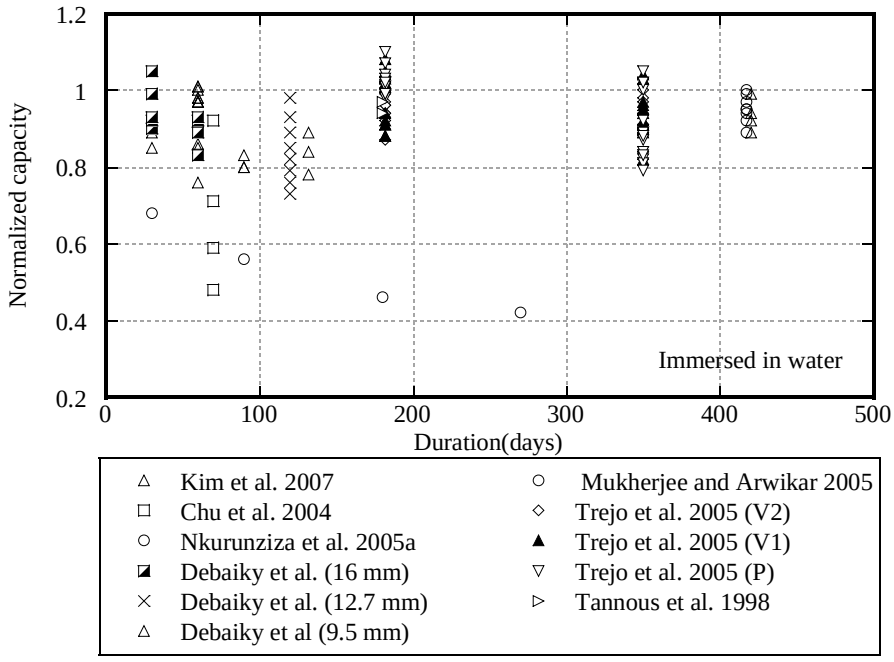

Fig. 1. Normalized residual tensile capacity of GFRP immersed in water

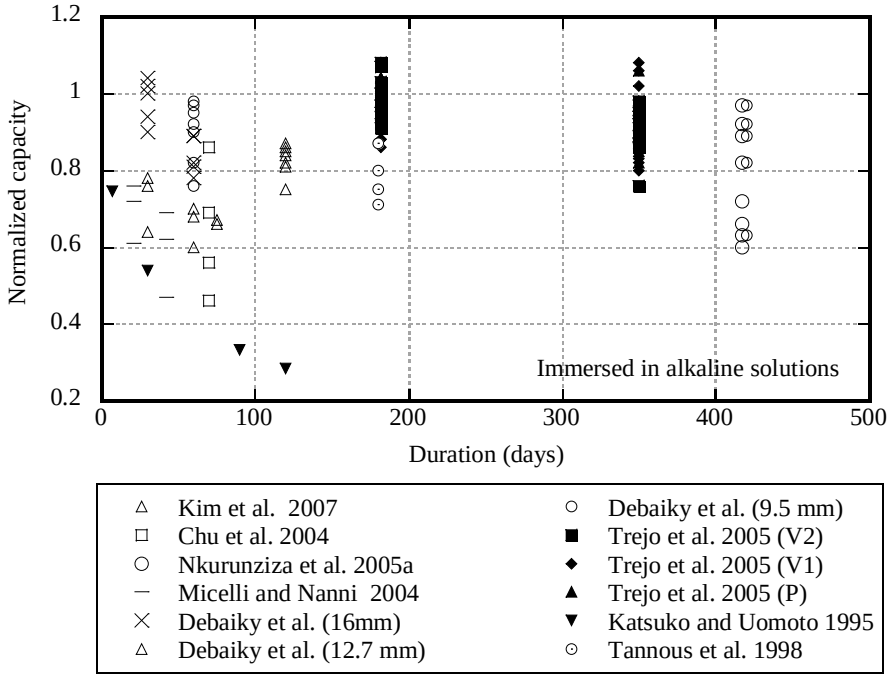

Fig. 2. Normalized residual tensile capacity in alkaline solutions

2.2. Deterioration of Tensile Capacity in Concrete

Because GFRP reinforcing bars are used as internal concrete reinforcement, it is more important to investigate the deterioration rate of GFRP bars when embedded in actual concrete environments. Tannous and Saadatmanesh (1998), Benmokrane et al. (2002), Chen et al. (2005), Mukherjee and Arwikar (2005), Almusallam et al. (2006), and Mufti et al. (2007) performed durability studies of embedded GFRP reinforcing bars in concrete.

In the studies performed by Tannous and Saadatmanesh (1998), several concrete beams were cast with GFRP bars made of the polyester and the vinylester resin. These GFRP bars had diameters of 10 mm (0.4 in.). All the concrete beams were saturated in

the solutions 1 and 2 made of 7 percent weight of $NaCl+CaCl_2$ (2:1 weight mixture) and $NaCl+MgCl_2$ (2:1 weight mixture), respectively. Ten concrete beams containing GFRP reinforcement were subjected to deicing salt solutions and tested in flexure to failure after zero, one, and two years of exposure. The GFRP reinforcement was then extracted from the beams and tension tests were performed to evaluate the residual properties. The measured losses in the tensile capacity of the GFRP bars made with polyester were 6 and 9.4 percent in solution 1 made of 7 percent weight of $NaCl+CaCl_2$ (2:1 weight mixture) and 10.6 and 12.8 percent in solution 2 made of 7 percent weight of $NaCl+MgCl_2$ (2:1 weight mixture) for one and two years of immersion, respectively. For GFRP bars made of vinylester resin, losses in tensile capacity were 6.5 and 9 percent in solution 1 and 8 and 11 percent when the GFRP reinforced concrete specimens immersed in solution 2, respectively. In the subsequent study performed by Tannous and Saadatmanesh (1999), for GFRP reinforcing bars made of AR glass losses in strength after 730 days immersed in $NaCl+CaCl_2$ and $NaCl+MgCl_2$ were 29.5 and 34.17 for polyester resin, and 30.98 and 28.21 for vinylester resin, respectively.

Mukherjee and Arwikar (2005) performed accelerated aging tests and natural environment tests to investigate the durability performance of the GFRP reinforcing bars embedded in concrete exposed to tropical environments. To accelerate testing, concrete beams were cast with GFRP reinforcement and loaded up to 50 percent of their ultimate strength. In this study, the sustained loading was applied to create cracks in the concrete and GFRP bars. One group of concrete beams was saturated in a water tank at $60^{o}C$

(140°F) for 3, 6, and 12 months. Some additional GFRP reinforcing bars were directly immersed in water and were used as control specimens. Another group of beams was stored outdoors for natural weathering in Bombay (India) after the immersion in water for 18 to 30 months. After conditioning, the GFRP reinforcing bars were removed from the concrete beams and tension tests were performed to assess the residual tensile strength. The reduction in the tensile strength of the outdoor conditioned GFRP specimens was 34.6 and 38.6 percent over 18 and 30 months, respectively. The reduction in the elastic modulus was relatively low. The authors reported that although the vinylester resin protects the glass fibers from alkali attack, deterioration under stress may occur due to the combined effect of exposure to the high temperature, moisture, and alkalis. In addition, the authors correlated reductions in tensile strength of GFRP exposed to water with the residual tensile strength of GFRP bars embedded in saturated concrete. It was concluded that the strength ratio of specimens exposed to water to specimens embedded in concrete was 32:1.

Almusallam et al. (2006) and Giernacky et al. (2002) investigated the longer-term durability behavior of GFRP reinforcement embedded in concrete beams under sustained loads. The type of GFRP bars was of E-glass with modified vinylester polymer with 60 percent volume fraction of E-glass fiber. A total of 36 concrete beams with embedded GFRP reinforcement were immersed in tap and sea water at an elevated temperature of 40°C (104°F) for up to 16 months. Concrete beams immersed in these environments were subjected to loads of 20 to 25 percent of ultimate tensile capacity. GFRP bars were extracted from the beams and tension tests were performed after 4, 8,

and 16 months of exposure. For the 16 month conditioning, reduction in the tensile capacity without loading and with loading was 16.3 and 47 percent in water and 19.6 and 48 percent in sea water, respectively. It is clear that degradation of the GFRP bar was significant when the bars were subjected to sustained loads. Giernacky et al. (2002) performed similar tests to estimate the deterioration of GFRP bars embedded in concrete. One group of GFRP reinforcement made with E-glass and vinylester resin was embedded in concrete beams and conditioned in a $Ca(OH)_2$ solution with a pH of 12.5 at $60\,^{o}C$ $(140\,^{o}F)$. The other group of GFRP bars was embedded in concrete and conditioned in the laboratory. A constant load of 20 percent of the ultimate tensile strength was applied to all specimens during conditioning. The reduction in the tensile capacity of the embedded GFRP bars after 60 days of immersion in the $Ca(OH)_2$ solution and stored in laboratory conditions for 180 days was 19.6 percent. However, the change in modulus of elasticity was negligible.

In research performed by Chen et al. (2005), GFRP bars were embedded in concrete. One set of GFRP reinforced specimens was immersed in a solution with a pH of 12.7 at $60\,^{o}C$ $(140\,^{o}F)$, while the other GFRP reinforced specimens were kept in a tap water tank at $20\,^{o}C$ $(68\,^{o}F)$ for 90 days. No loads placed on the concrete beams. The experiments showed a 9.6 and 38.8 percent reduction in tensile capacity for specimens immersed in tap water and simulated concrete pore solution, respectively.

An investigation was initiated to address the issue related to the in-situ alkali resistance of GFRP reinforcing bars (Mufti et al. 2007). Concrete specimens reinforced with GFRP bars were extracted from five different demonstration structures located in

North America. GFRP bars made with E-glass and vinylester resin were embedded in concrete for 5 to 8 years and exposed to a wide range of environmental conditions. These samples were extracted from actual structures and sent to different research laboratories to perform analysis on the physical and chemical composition of the bars. All research laboratories concluded that there was no degradation of the GFRP bars embedded in the concrete structures. However, it should be noted that no mechanical tests were conducted to assess potential loss in capacity. In addition, the researchers performed energy dispersive x-ray test analysis near the center of the glass fibers instead of near the edge of bar-concrete interface where deterioration would be expected.

Bakis et al. (2005) investigated the difference in the deterioration rate of GFRP bars between simulated pore solution and actual concrete under loads. GFRP bars made of E-glass and vinyl ester resin were embedded in the concrete beams. After pre-cracking, specimens were placed in four separate environmental conditions for specific conditioning period. After completing sustained loading, the beams were unloaded and subjected to tension tests to measure the residual tensile capacity. Change in tensile strength of bars embedded in concrete beams was 2.5 percent less than the controlled bars that were neither cast in concrete nor loaded. However, reduction in tensile strength of GFRP bars immersed in $Ca(OH)_2$ was nearly 25 percent in one year. It was concluded that reduction in the tensile capacity in real concrete condition is much less than the reduction with simulated pore solution.

The deterioration rate of GFRP reinforcement in actual concrete environments is summarized in Table 3 and 4 and plotted in Fig. 3.

Table 3. Summary of the deterioration of GFRP (vinylester) in concrete

Bar Types (matrix /glass)	Bar Diameter mm (inch)	Conditioning (immersion in)	Saturated or Not	Exposure Temp. ^{o}C (^{o}F)	Exposure Duration (days)	Applied Stress (%)	Capacity Loss (%)	Reference
modified vinylester/ E-glass	10 (0.4)	water	saturated	40 (104)	480	0	16.29	almusallam et al. 2006
				40 (104)	480	20-25	47.1	
	10 (0.4)	water		40 (104)	480	0	19.65	
				40 (104)	480	20-25	47.91	
vinylester/ E-glass	9 (0.3)			20 (68)	582	0	43.38	Dejke, 2001
				40 (104)	245		43.96	
vinylester/ E-glass	9.53 (0.38)	water	saturated	20 (68)	90	0	9.62	Chen et al. 2005
		alkaline solution (pH=12.7)		60 (140)	90		38.81	
vinylester/ E-glass	10 (0.4)	control specimen	dry concrete		365	0	3,56	Tannous and Saadatmanesh 1998
		NaCl+CaCl2 (2:1)	saturated		730		9.1	
		NaCl+MgCl2 (2:1)			730		11.05	
vinylester/ E-glass	9.5 (0.37)	water tank/cut out from beam	saturated	60 (140)	360	20	64.98	Mukherjee and Arwikar 2005
		outdoor /cut out from beam		outdoor	900		38.6	
vinylester/ E-glass		alkaline solution (pH=13.1)	saturated	22 (71.6)	140	30	16.07	Benmokrane et al. 2002
vinylester/ AR-glass	9.3 (0.37)						1.17	
vinylester/ AR-glass	10 (0.4)	control specimen	dry concrete		365	0	14.18	Tannous and Saadatmanesh 1999
		NaCl+CaCl2 (2:1)	saturated		730		30.98	
		NaCl+MgCl2 (2:1)			730		28.21	

(Modified vinylester: 60 % volume fraction of E-glass fiber, Almusallam et al. 2006)

Table 4. Summary of the deterioration of GFRP (polyester) in concrete

Bar Types (matrix /glass)	Bar Diameter mm (inch)	Conditioning (immersion in)	Saturated or Not	Exposure Temp. ^{o}C (^{o}F)	Exposure Duration (days)	Applied Stress (%)	Capacity Loss (%)	Reference
polyester/ E-glass	10 (0.4)	control specimen	no		365	0	3.81	Tannous and Saadatmanesh 1998
		NaCl+CaCl2 (2:1)	yes		730		9.43	
		NaCl+MgCl2 (2:1)			730		12.81	
polyester/ AR-glass	10 (0.4)	control specimen	no		365	0	7.34	Tannous and Saadatmanesh 1999
		NaCl+CaCl2 (2:1)	yes		730		29.5	
		NaCl+MgCl2 (2:1)			730		34.17	

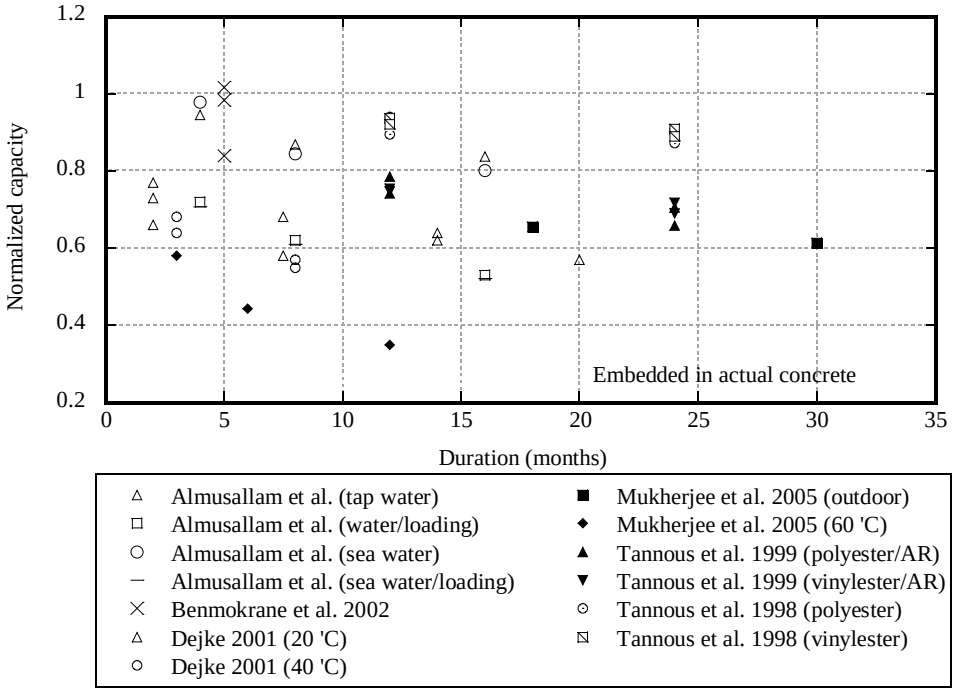

Fig. 3. Normalized residual tensile capacity in concrete

2.3. Comparison of Deterioration between Solutions and Concrete

In previous studies GFRP reinforcement was exposed to simulated concrete pore solutions and embedded in actual concrete beams to estimate the durability of these GFRP bars in concrete environments. In general, the deterioration rate of GFRP exposed to simulated pore solutions was much faster than that of GFRP exposed to actual concrete environment.

For the GFRP bars made of vinylester resin, the highest reduction in the tensile capacity of the GFRP bars immersed in alkaline solution (pH=11.5) was 53.7 percent for 70 days exposure (Chu et al. 2004). In water immersion, the maximum reduction in the tensile strength of GFRP bars was measured to be 57.7 percent for 270 days conditioning (Mukherjee and Arwikar 2005). Reduction in tensile strength of the GFRP bars embedded in actual concrete was 48 percent for 480 days immersion in sea water under 20 to 25 percent sustained stress (Almusallam et al. 2006) and 65 percent for 360 days immersion in water tank at temperature 60 (140) combined with 20 percent stress (Mukherjee and Arwikar 2005). Chen et al. (2005) reported that the reduction in the tensile strength of the extracted GFRP bars from concrete beams immersed in alkaline solution (pH=12.7) for 90 days was 38.8 percent without sustained stress.

2.4. Prediction Model for Longer-Term Performance of GFRP Bars

The Arrhenius principle is widely used to predict the degradation of mechanical properties of GFRP reinforcement as a function of temperature. Accelerated aging tests and prediction modeling based on the Arrhenius relationship have been developed by Litherland et al (1981). This assumes that the material's behavior at higher temperatures can be extrapolated to lower temperatures of practical interest in the field (Iskander and Hassan 2001). It has been reported that using accelerated aging tests at different temperatures, the time rate of deterioration at an average service temperature can be predicted. If the rate of change in mechanical properties at higher temperatures is known, the service life of materials in the field can be predicted (Bank et al. 2003).

An approach using the Arrhenius' principle was performed by Katsuki and Uomoto (1995), Vijay and Gangarao (1999), Dejke (2001), Chu et al. (2004), and Chen et al. (2005). Katsuki and Uomoto (1995) reported that the Arrhenius equation offers a good correlation between the temperature and the rate of diffusivity and deterioration of the GFRP bars. By using the Arrhenius equation, the influence of temperature on the diffusion coefficient at some temperature can be determined with diffusion coefficients at different temperatures, D_0 and D_t. The Arrhenius equation can be shown as follows:

$$D_t = D_0 \exp\left(\frac{-E_d}{RT}\right) \tag{1}$$

where D_t is the apparent diffusion coefficients at temperature T (Kelvin). The activation energy for diffusion, E_d, provides an convenient indication of the energy

barrier that has to be overcome for diffusion of moisture to take place (Chu et al. 2004). R is the universal gas constant (8.3143 J/mol·K).

Dejke (2001) proposed that the relative time shift factor (TSF) can be used to transform the time in the accelerated testing to real service lives of GFRP reinforcing bars. As the time for a certain reaction to take place must be proportional to the inverse of the rate of reaction, Dejke (2001) reported determining the TSF as follows:

$$\text{TSF} = \frac{t_1}{t_2} = \frac{c/k_1}{c/k_2} = \exp\left[\frac{E_d}{R}\left(\frac{1}{T_1} - \frac{1}{T_2}\right)\right] \tag{2}$$

where T_1 and T_2 are the exposure temperatures (in Kelvin), and t_1 and t_2 are the times required for a certain decrease in some mechanical properties at temperatures T_1 and T_2, respectively. Dejke (2001) indicated that by using the Arrhenius plot of the strength retention curves of different exposure temperatures, the relationship between time and temperature can be determined as a logarithmic time scale and expressed as straight parallel lines. This indicates that the degradation of tensile strength is proportional to the logarithmic time scale at all temperatures. By using Equation (2), the TSF can be described, and Dejke (2001) proposed that the service life can be predicted using the *TSF* from the target temperature and time values required for specific strength loss.

Using the Arrhenius principle, Vijay and Gangarao (1999) proposed the following model to correlate the accelerated aging lab tests with actual aging in the field:

$$\frac{N}{C} = 0.098 * \exp\left(0.0558 * T\right) \tag{3}$$

where N is the actual age in natural days, C is the days of accelerated ages in laboratory, and T is the temperature of conditioning in the laboratory (^{o}F). However, Nkurunziza et al. (2005b) reported that this prediction model is based on the Northeastern climate conditions (i.e., West Virginia), where the average annual temperature is 11.7^{o}C (53^{o}F). With this equation (3), 104 days of exposure in the laboratory at 60^{o}C (140^{o}F) is equivalent to 69 years of service life in a standard concrete environment at 11.7^{o}C (53^{o}F). Although there are many advantages of using the Arrhenius equation for predicting the longer-term performance of GFRP bars, Iskander and Hassan (2001) indicated that Arrhenius modeling of solid structures has a number of limitations. Firstly, Arrhenius principle assumes that reaction between all the molecules and aggressive media is subjected to take place freely. However structural members are usually exposed to aggressive media at the surface only. Secondly, more than one deterioration mechanism may cause reduction in mechanical, chemical, and physical properties of GFRP bars over a wide range of temperatures.

Tannous and Saadatmanesh (1998) reported that Fick's Law and the Langmuir two-phase model can be used to model the moisture diffusion in composites. The authors reported that Fick's Law is appropriate to predict the changes in the moisture uptake and the residual strength of GFRP bars exposed to simulated pore solution. The authors reported that diffusion coefficient, D , can be estimated using experimental data as follows (Shen and Springer 1976):

$$D = \frac{\pi r^2}{16}\left(\frac{M_2 - M_1}{M_m}\right)^2\left(\frac{1}{\sqrt{t_2} - \sqrt{t_1}}\right)^2 \quad (4)$$

where M_1 and M_2 are the percent moisture contents of the GFRP reinforcing bar at times t_1 and t_2, respectively, M_m is the moisture content at saturation, and r is the radius of the GFRP reinforcing bar. It was assumed that the tensile strength of GFRP bar can be calculated quantitatively by detecting the alkali penetration area into the bar (Katsuki and Uomoto 1995). The diffusion coefficient, D, in Equation (4) can be used to determine the depth of penetration, x, of pore solution as follows:

$$x = \sqrt{2DCt} \tag{5}$$

where C is the normalized or relative alkaline concentration (mol/l) and t indicates the curing time (hrs). Using the Equations (4) and (5), the residual tensile strength, P_r at time t, was estimated as follows (Tannous and Saadatmanesh 1998):

$$P_r = P_0\left(1-\frac{x}{r}\right)^2 = P_0\left(1-\frac{\sqrt{2DCt}}{r}\right)^2 \tag{6}$$

where, P_0, P_r are the initial and residual tensile strengths of the GFRP reinforcing bars and r is the radius of the bar.

However, debate still exists about using this equation to estimate the residual tensile strength of GFRP in longer-term field exposure conditions (i.e., in concrete). The main issue with exposing GFRP bars to simulated pore solution is that concrete pores are rarely constantly saturated, especially in bridge decks. The depth of penetration of moisture into the GFRP bars using pore solution penetration assumption likely overestimates the actual depth of penetration when the GFRP bars are embedded in concrete, resulting in a less severe loss of strength. Grasley et al. (2003) reported that

the moisture content near the concrete surface exhibits significant reductions as the depth increases, even shortly after casting. There is a need to correlate the results from the accelerated tests with the results from actual concrete exposure conditions.

The second issue concerning the use of this methodology is that the equation assumes that all the glass fibers exposed to pore-solution contribute nothing to the residual tensile strength. This assumes that immediately after the glass fiber is exposed to the exposure solution, the glass fiber looses all ability to contribute to the tensile strength. However, Trejo et al. (2005) suggested that this is not accurate, because when the glass fiber contacts with the alkaline concrete pore solution, reduction in tensile strength do not occur immediately, but is time dependent. To account for the fact that the degradation rate of GFRP bars in concrete is not instant, a modified prediction model including the reduction factor, λ, was proposed as follows:

$$\sigma_t = \left(1 - \frac{\sqrt{2D\lambda t}}{r}\right)^2 \sigma_0 \tag{7}$$

where λ is the reduction factor and is a function of time and the normalized alkaline concentration, $\lambda = f(C,t)$. σ_0 and σ_t are the tensile strength before exposure and at time t, respectively.

Trejo et al. (2005) reported that the residual strength of GFRP bars can be computed using average diffusion coefficients from exposed specimens to distilled water. In addition, the value of λ could be obtained by fitting the predicted residual tensile strength to the overall lowest observed tensile strength (at 0 to 50 weeks exposure times) by using least squares. However, it should be noted that there are obvious

limitations on the ability of a model to predict residual tensile strength at long periods of times due to the data for exposure of only one year. As a result, there is need to determine the value of λ for GFRP bars embedded in concrete, exposed to exterior weather conditions and exposed to loading. In addition, the validity of prediction model should be evaluated.

2.5. Design Requirements

American Concrete Institute (ACI 2007) Committee 440 and the American Association of State Highway and Transportation Officials Load and Resistance Factor Design (AASHTO LRFD 2008) proposed the design recommendations and specification as a guide for design and construction of the GFRP reinforced concrete system. Design recommendations are on the basis of the current information or knowledge obtained from experimental research and actual field applications. In addition to existing codes and guidelines, this document provides engineers with support in the specifications, design and construction of concrete structures containing the FRP reinforcement.

ACI 440 and AASHTO design provisions are based on the limit state design principles in that an FRP reinforced concrete member is designed to satisfy the required strength and then checked for fatigue and creep ruptures and serviceability criteria. In many occasions, serviceability criteria and fatigue and creep rupture limits may control the design of flexural concrete members reinforced with FRP bars.

ACI 440 design guidelines addresses that the use of FPR reinforcing bars for concrete structures needs the development of design procedures to guarantee appropriate safety from failure. Unlike conventional steel reinforcing bars, FRP materials respond

linearly and elastically to failure at which point brittle rupture occurs and linear stress versus strain relationship to failure must be used. Because FRP reinforced concrete members would not exhibit ductility as is commonly observed for steel reinforced concrete members, the design of concrete structures containing FRP bars should take into account the mechanical performance of FRP materials. It was recommended that the lower flexural capacity reduction factor might be required to be compatible with the specific performance limitations of FRP materials.

In general design consideration of ACI 440 and AASHTO specifications, because long-term exposure to various types of environment can reduce the tensile strength of FRP bars, ACI 440 and AASHTO reported that material properties used in design equations should be reduced based on the types and level of environmental exposure. The design tensile strength of the GFRP reinforcing bar considering reductions for service environment is determined as:

$$f_{fu} = C_E f_{fu}^* \tag{8}$$

where f_{fu} is the design tensile strength of the GFRP considering reductions for the service environment, C_E is the environmental reduction factor for various fiber type and exposure conditions, and f_{fu}^* is the guaranteed design tensile strength of the GFRP bar. The guaranteed design tensile strength is defined as the mean tensile strength of a sample of test specimens minus three times the standard deviation ($f_{fu}^* = f_{u,ave} - 3\sigma$). Table 5 shows the environmental reduction factors recommended by ACI 440 and AASHTO Specifications.

Table 5. Environmental reduction factor

Exposure Condition	Environmental Reduction Factor
Concrete not exposed to earth and weather	0.8
Concrete exposed to earth and weather	0.7

Based on the durability of each fiber type, the environmental reduction factors shown in Table 5 are conservative estimates and are on the basis of general view of Committee 440. The environmental reduction factors include the temperature effects. However, it is noted that this reduction factor should not be used in environments with higher temperature than glass transition temperature (T_g) of resin of the FRP bars.

3. EXPERIMENTAL PROGRAM

In the previous study conducted by Trejo et al. (2005), 36 concrete beams were cast and tested. This beams, containing three different GFRP types (V1, V2, and P) with different diameters 16 and 19 mm (0.625 and 0.75 inch) of GFRP reinforcing bars were exposed to outside environmental conditions for over seven years. The dimensions of the concrete beams were 3000 mm (120 inch) long by 420 mm (16.5 inch) wide by 200 mm (7.87 inch) depth. The GFRP reinforcing bars were placed with three different cover depth (2.5, 5, and 7.5 mm [1, 2, and 3 inch]) on the tension side of the beams. The beams were loaded to failure. After the bending tests, the concrete beams were exposed to outdoor conditions for over seven years at the Riverside Campus of Texas A&M University in College Station, Texas as shown in Fig. 4 The mean annual temperature was $23^{o}C$ ($69^{o}F$) and the mean annual precipitation was 1008 mm (39.7 inch). The minimum and maximum average daily temperatures were $5^{o}C$ ($40^{o}F$) and $40^{o}C$ ($96^{o}F$), respectively. Bars that were not embedded in concrete or exposed to solutions were used as control specimens.

Fig. 4. Concrete beams containing the GFRP reinforcement at the Riverside Campus in Texas A&M University

In this study, the GFRP bars embedded in the concrete were extracted and used to evaluate the longer-term performance of the GFRP bars. Tension tests were carried out to measure the residual tensile capacity and change in elastic modulus. In addition, the exposed GFRP reinforcing bars were characterized using Scanning Electron Microscopy (SEM), Energy Disperse X-Ray (EDX), Fourier Transform Infrared Spectroscopy (FTIR), Differential Scanning Calorimetric (DSC) and Thermo-gravimetric Analysis (TGA) tests. The concrete was characterized for alkalinity, void content, and density. Because the concrete beams were initially subjected to a four point bending tests, a preliminary assessment was needed to determine if the bending tests affected the residual tensile strength of the GFRP bars embedded in the concrete. This preliminary assessment will be presented later.

3.1. Materials

Trejo et al. (2005) provided the properties of the GFRP reinforcing bars with diameters of 16 and 19 mm (0.63 and 0.75 inch). The three different bar types were identified as bar V1, V2, and P, representing bars produced by Hughes Brothers, Pultrall, and Marshall Industries, respectively. Fig. 5 shows the surface of each bar type.

Fig. 5. Surface of each GFRP (V1, V2, and P respectively)

Schaefer (2002) reported that bar type V1 consists of an external helical fiber wrapping and a fine sand aggregate with a circular cross section. The bar is composed of E-glass fibers embedded in a vinyl ester resin. Bar type V2 consists of a surface with a coarse sand coating and a circular cross section. This bar is made of vinyl ester resin and E-glass fibers. Bar type P is made with E-glass fibers and a polyethylene terephthalate (PET) polyester resin. The surface of the bar is smooth and contained ribs similar to conventional steel reinforcement. Trejo et al. (2005) also provided the range of diffusion coefficients for the different types of GFRP bars as shown in Table 6. The

diffusion coefficient was reported to have a mean value of 8×10^{-13} mm^2/sec (1.38×10^{-9} inch^2/sec) and a standard deviation of 3.52×10^{-13} mm^2/sec (0.54×10^{-9} inch^2/sec). These values are used for modeling in this paper.

Table 6. Diffusion coefficients (Trejo et al. 2005)

Bar type	Diameter mm (inch)	Distilled water mm^2/sec (inch^2/sec)	Alkaline solution mm^2/sec (inch^2/sec)
V1	16 (0.63)	2.88E-13 (4.46E-16)	6.58E-13 (1.02E-15)
	19 (0.75)	1.12E-12 (1.74E-15)	1.54E-12 (2.39E-15)
V2	16 (0.63)	7.35E-13 (1.14E-15)	7.68E-13 (1.19E-15)
	19 (0.75)	5.18E-13 (8.03E-16)	1.19E-12 (1.84E-15)
P	16 (0.63)	1.06E-12 (1.64E-15)	6.71E-13 (1.04E-15)
	19 (0.75)	1.24E-12 (1.92E-15)	8.71E-13 (1.35E-15)
Average		8.27E-13 (1.28E-15)	9.05E-13 (1.47E-15)
Standard Deviation		3.76E-13 (5.82E-16)	3.49E-13 (5.41E-16)
Average (for all data)		8.9E-13 (1.38E-15)	
Standard Deviation (for all data)		3.5E-13 (5.43E-16)	

3.2. Preliminary Tests

The concrete beams containing the GFRP bars were initially subjected to a four point bending tests. The bending tests set up and bar layout are shown in Figs. 6 through 7.

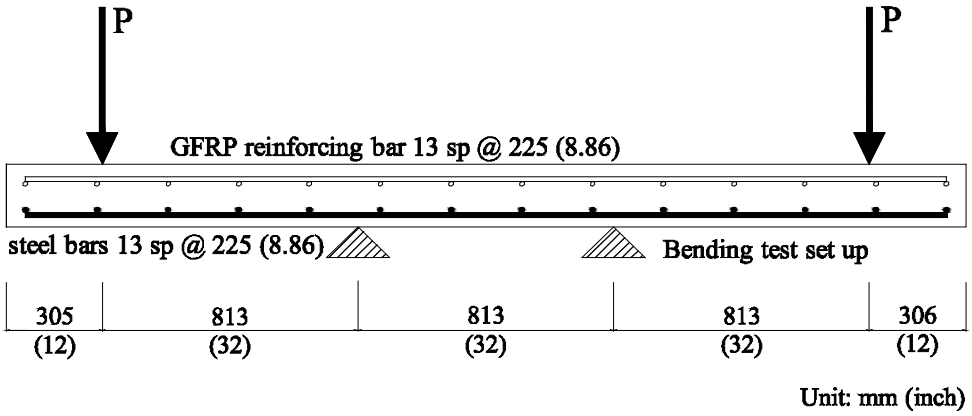

Fig. 6. Bending test

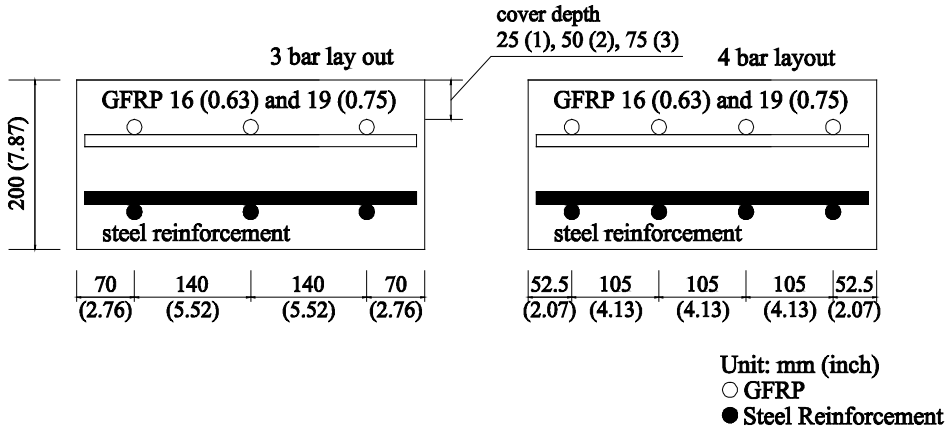

Fig. 7. GFRP specimen and bar layout

The research team had concerns that the initial bending test might have reduced the ultimate tensile capacity of the embedded GFRP reinforcing bars. To determine if

the beam bending test affected the ultimate tensile strength of the GFRP bars, preliminary tension tests were performed using 60 control bars with two loading types. It was determined that a preload of 66.72 kN (15 kips) would represent the stress in the bars caused by the initial four point bending tests. For each bar type and bar diameter ten tensile specimens were fabricated. Of the ten samples, five were preloaded to 66.72 kN (15 kips), unloaded, and loaded again until failure. This loading type simulated the initial stresses caused by the bending during the actual four point beam testing. The second set of five bars was loaded directly to failure.

3.3. Tension Tests

When extracting the GFRP bars from the concrete beams, care was taken not to damage any area of the bars. Each bar was examined and sections of the bar that were undamaged were set aside for testing. One hundred and sixty specimens were available for testing; the number of tests for each bar type is summarized in Table 7.

Table 7. Available specimen with nominal cover depth

Bar Type	Bar Size mm (inch)	25 mm (1 inch) Cover	50 mm (2 inch) Cover	75 mm (3 inch) Cover	Number of Bars Extracted
V1	16 (0.63)	10	14	11	35
	19 (0.75)	9	10	10	29
V2	16 (0.63)	10	10	10	30
	19 (0.75)	8	5	5	18
P	16 (0.63)	5	5	5	15
	19 (0.75)	11	11	11	33
Total		47	45	45	160

An effort was made to be consistent with the test methods performed by Trejo et al. (2005) since data was to be compared. The GFRP bars were cut into 1040 mm (41 inch) lengths, avoiding any physical damage that may have resulted during extraction. Steel pipe, 38 mm (1.5 inch) in diameter, was cut into 305 mm (12 inch) sections and these were used for grips. The grips are necessary when testing GFRP bars to prevent damage to the GFRP bar ends. The GFRP bars were centered in the steel pipe grips. This prevented any bending that could occur during testing. The GFRP bars were grouted into the pipe grips with a high-performance expansive grout. After curing for a minimum of 24 hours, the specimens were placed in the testing apparatus. A small load was applied to set the grips prior to final tightening of the connections between the pipe and machine grips. A LVDT was mounted to the specimen and the bars were loaded to failure. A loading rate of 2.8 mm/min. (0.11 inch/min.) was used. A 489 kN (110 kips) load frame with a 0.5 percent load accuracy (within the range tested) was used. Fig. 8 shows the test specimen and the grip system.

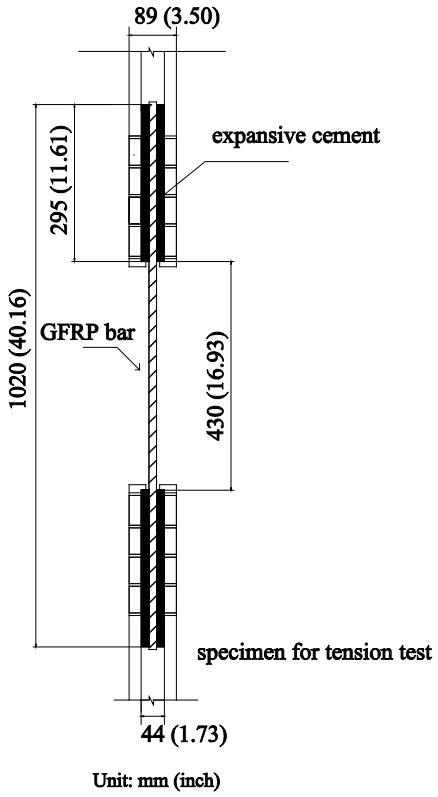

Fig. 8. Specimen layout showing grip system

3.4. Modulus of Elasticity Tests

The modulus of elasticity (MOE) is important as it plays a large role in affecting crack widths, deflections, and other design requirements for reinforced concrete structures (Nkurunziza et al. 2005a). Although most of the literature indicates that the MOE does not decrease as a function of time, tests were performed because data for GFRP bars embedded in concrete for 7 years was not available. The MOE values for the GFRP bars were obtained from data collected during the tensile testing. The results from this test will provide information on the long-term effects on the modulus of elasticity of GFRP bars embedded in concrete. An extensometer with three LVDTs was used to measure

and to collect strain data. Fig. 9 shows the extensometer being mounted to GFRP bars (left) and close-up of LVDTs (right).

Fig. 9. LVDTs being mounted to GFRP bar (left) and LVDT for MOE (right)

The device consists of two parallel round plates with three LVDTs positioned perpendicular in holes on the plates. One end of the LVDT was fixed while the other end was free move up to down. The three LVDTs were positioned at 120° and the strain from all LVDTs was averaged to determine the strain. Three LVDTs were used to account for any bending that could occur in the bar during testing. The measured gage length was 67 mm (2.64 inch). LVDTs were used with the data acquisition system. As recommended by ACI 440.3R-04, the equation for the modulus of elasticity is as follows,

$$E_L = \frac{F_1 - F_2}{(\varepsilon_1 - \varepsilon_2) A} \tag{9}$$

where E_L is the axial (longitudinal) modulus of elasticity, MPa, A is the cross sectional area, mm^2, F_1 and ε_1 are the load and corresponding strain, respectively, at approximately 50 percent of the ultimate tensile capacity or guaranteed tensile capacity, N and dimensionless, respectively; and F_2 and ε_2 are the load and corresponding strain, respectively, at approximately 20 percent of the tensile capacity or guaranteed tensile capacity, N and dimensionless, respectively. Data was taken from the same specimens that were used for the tension tests. Before beginning the tests, the LVDTs were fixed on the bar. The extensometer was not removed until the failure of GFRP occurred.

3.5. GFRP Characterization Tests

Because one of the main purposes of this study is to evaluate the mechanical properties of GFRP bars embedded in concrete, it is necessary to characterize both the GFRP bars and the concrete of the beams. Several physical tests were performed to characterize or confirm several properties of GFRP bar and the concrete. The GFRP bars were characterized using SEM, EDX, FTIR, DSC, and TGA tests.

SEM was conducted to visually identify possible signs of deterioration in the GFRP reinforcing bars. A JEOL 6400-SEM with a resolution and maximum acceleration voltage of 3.5 nm and 20 kV was used, respectively. The specimens for the SEM test were prepared by cutting, mounting in resin, polishing. EDX was run in conjunction with the SEM test to identify elements in the GFRP reinforcing bars and to confirm the types of glass fibers used in this study. It was reported that the GFRP bars contain E-glass, if zirconium (Zr) is not detected in EDX test (Mufti et al. 2007).

As EDX cannot detect the hydroxyl ions (OH^-) or elements lighter than sodium (Na), FTIR tests were performed to investigate the changes in the elements in polymer resin focusing on OH^- and C-H groups in the GFRP reinforcing bars. Scheirs (2000) reported that FTIR is useful in accessing whether the material has degraded and for determining the mechanism of degradation. When the GFRP reinforcing bars are embedded in concrete, alkali hydrolysis that is the deterioration mechanism of the resin linkage may take place due to the high alkaline environment in concrete. During the hydrolysis reaction, hydroxyl groups induce into GFRP bars and resin chain may be broken (Mufti et al. 2007). Changes in the amount of hydroxyl groups close to resin matrix of the composite material were investigated using FTIR.

DSC determines the amount of heat transferred to the GFRP bars. Mufti et al. (2007) proposed that the transition temperature is an important physical property of the matrix, not only as an indicator of thermal stability, but also as an indicator of the structure of the polymer and its remaining mechanical properties. DSC tests were performed using a TA Instrument Q100. Each powdered sample was sealed in an aluminum pan place in the instrument and the temperature was increased and subsequently decreased at a rate of $10\,^{o}\mathrm{C}/\min\,(50\,^{o}\mathrm{F}/\min)$ from 25 to $200\,^{o}\mathrm{C}$ (77 to $392\,^{o}\mathrm{F}$) under the constant flow of dry nitrogen. Values were obtained from the second heating cycle.

TGA was performed to determine the fiber volume fraction in the GFRP reinforcement. Specimens were cut into pieces with a weight of approximately 10 to 100 mg (2.2×10^{-4} lb) and were heated to $627\,^{o}C$ ($1160.6\,^{o}\mathrm{F}$), burning away the resin

matrix and leaving the glass fibers until the weight change was less than 0.05 percent. This rids the GFRP of the polymer matrix and the resulting mass is the mass of the glass fibers (Dejke 2001).

3.6. Concrete Characterization Tests

It has been reported that GFRP reinforcing bars embedded in concrete are susceptible to the highly alkaline pore solution present in concrete. This can lead to a reduction in tensile strength and possible reduction in the elastic modulus (Ceroni et al. 2006). The issue of how alkalinity levels affect the deterioration and longer-term performance of these bars needs to be addressed and possibly represented in a newly developed model. In this study, the concrete was characterized using pH, void, density, and absorption test.

To assess the alkalinity of the concrete, the Environmental Protection Agency (EPA) test method 9045D was used to obtain the pH values of the concrete pore solution. Concrete specimens were initially crushed in a pestle. A uniform powder was attained using a #20 sieve. Approximately 20 grams (0.044 lb) of concrete powder and 20 ml (0.68 oz) of distilled water were mixed. The mixture was covered and stirred with a mixing pad for five minutes. After mixing, the suspension was left to settle for 15 minutes before the pH reading was taken. A Denver Instrument model 250 pH meters with a Denver Instrument pH electrode was used to evaluate the pH. The objective of alkalinity tests is to assess the pH and to determine if the reduction of the tensile capacity is related to the alkalinity of concrete pore solutions.

Because the exposure of the GFRP bars to moistures may play a major part in the deterioration of GFRP bars, it was clear that the quantity of permeable voids in the

concrete would also be important. The literature reported that moisture intake by GFRP bars can results in changes in properties of the bars (Katsuki and Uomoto 1995). Nkurunziza et al. (2005a) suggested that the modulus and stress transfer can be affected by an increase in crack density, absorption, and void percentage in the concrete. ASTM Standard C 642-97 was followed to determine the void content, density, and absorption of the concrete. Concrete cores were extracted using a 101.6 mm (4 inch) diameter coring bit.

3.7. Analysis of Potential Influencing Factors

Several factors were considered as possibly influencing the capacity of GFRP bars. These factors included concrete cover depth, concrete pore solution pH, concrete porosity, and concrete beam storage position. The data obtained from the tension tests was normalized with respect to the average “as received” tensile strength to investigate the relationship between the residual tensile capacity and the influencing factors, regardless of the physical properties of the bar.

4. EXPERIMENTAL RESULTS AND DISCUSSION

4.1. Preliminary Test Results

Analysis of the results from the preliminary tension tests showed that the beam bending tests had no effect on the ultimate tensile strength of the GFRP bar. Based on the statistical T-test of equality at a 0.05 level of significance, the hypothesis that the mean tensile strength for the preloaded bars is the same as the mean tensile strength for the non-preloaded bars cannot be determined to be different values. In other words, there is not sufficient statistical evidence to reject the hypothesis that both mean values of tensile strength for preloaded and for non-preloaded bars are different. Hence, it is concluded that the bending test did not affect the ultimate tensile properties of embedded bars. It should be noted that although the beam testing did not affect the ultimate capacity of the GFRP bars, the loading likely led to cracking in the bar's polymer matrix. Because cracking does lead to accelerated penetration of moistures, this preloading likely influenced the rate of strength loss. This cracked condition would be typical of structures that exhibit active loading, similar to bridge decks. This condition may not represent conditions where the bars experience relatively minor loads and no cracking in the polymer matrix. However, designers may not know whether a GFRP bar would exhibit at the polymer matrix and thus using the residual capacity of the GFRP bars with a cracked polymer matrix would be an appropriate approach.

4.2. Tension Test Results

As literature indicates the residual tensile strength of the extracted GFRP bars from concrete was noticeably reduced as compared to the tensile strength of control reinforcing bars. A comparison between the residual tensile strength of extracted and control bars was performed to evaluate changes in the mechanical properties, based on the type and size of the GFRP bars. Fig. 10 shows the tensile capacity for the extracted GFRP bars with and without exposures as a function of bar type and size. Table 8, 9, and 10 show the tensile strength results for the three different bar types. In all cases the mean bar capacity decreased as a function of time, indicating that the tensile capacity of GFRP bars is reduced when embedded in concrete. Of more importance is the rate at which the capacity of these bars decreases and how these rate correlates with design parameters. These issues will be addressed in section 5 on modeling. The following sections attempt to identify other variables that influenced the reduction in capacities of the GFRP bars.

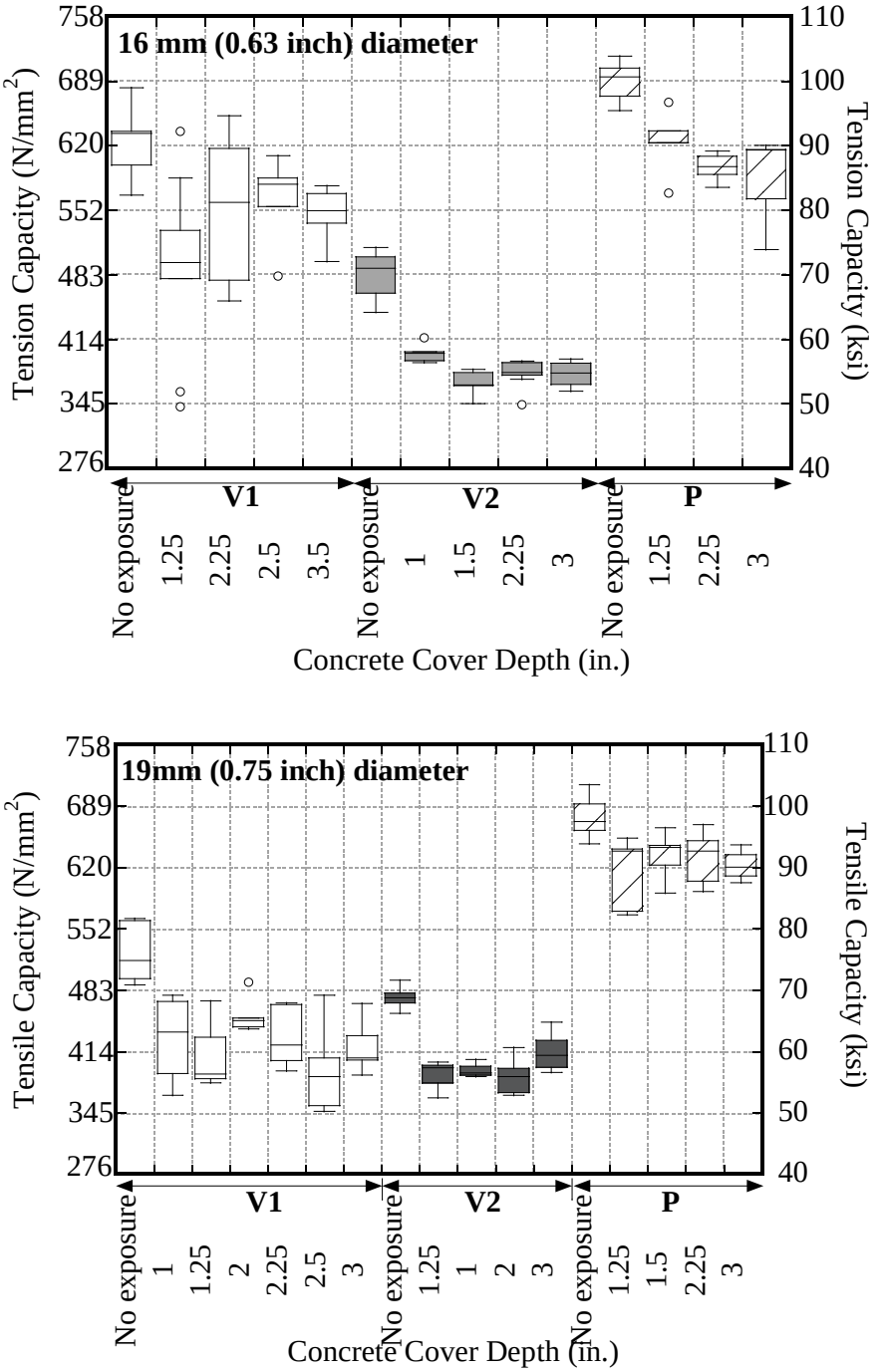

Fig. 10. Comparison tensile capacity of GFRP bars (16 and 19 mm diameter)

The figures separate data according to the cover depth that was measured when the bars were extracted. For both GFRP reinforcing bar sizes, all bars showed a reduction in tensile strength when compared with the control bars. In addition, the results showed that the cover depth is not an influencing parameter for deterioration of the tensile strength.

Based on the average values of the tensile strength of the extracted bars, regardless of cover depth and preload, the reduction of tensile strength of the type V1 bars with 16 mm (0.63 inch) and 19 mm (0.75 inch) diameter size was 12.7 and 21.0 percent over the control bars, respectively. The tensile strength loss of the type V2 bars for the16 mm (0.63 inch) and 19 mm (0.75 inch) diameters was reduced by 23.5 and 16.3 percent of the control bar, respectively. In the case of the type P bars, the 16 mm (0.63 inch) and 19 mm (0.75 inch) bars exhibited reduction in tensile strength of as 12.8 and 7.8 percent, respectively.

As already noted, the type V1 bars are made with external helical fiber wrapping with an average spacing of 26.4mm (1.04 inch) (Schaefer, 2002). When the tension test was conducted it was found that the failure initially occurred at the helical wrapping as shown in Fig.11.

Fig. 11. Failure Initiation of bar type V1

Benmokrane et al. (2002) reported that initiation of failure of the type V1 bars occurs at wrapping area, because the glass fibers of the type V1 located in wrapping zone are squeezed by the compression of helical wrapping and are also not well protected by the resin from the penetration of alkaline solution.

The literature reported that vinyl ester exhibited lower diffusivity and higher resistance to alkaline and chemical attack than polyester resin (Tannous and Saadatmanesh 1998). However, it was found that reductions in tensile strength of GFRP bars made of the polyester resin was less than the that of GFRP bars made of vinylester resin. It was inferred that reduction in the tensile strength of the GFRP bars embedded in longer-term duration in concrete would be dominated by combined deterioration mechanism caused by environmental factors influencing on durability rather than affected by only the diffusivity of the resin matrix of the GFRP bars. Table 8 through 10 show the tensile strength results for the three different bar types.

Table 8. Tension test results for extracted V1 type GFRP bars (#5 and #6)

V1 #5		V1 #6	
Tensile Strength No Exposure ksi (MPa)	Tensile Strength – After Exposure ksi (MPa)	Tensile Strength No Exposure ksi (MPa)	Tensile Strength After Exposure ksi (MPa)
76.39 (526.71)	70.31 (484.78)	83.28 (574.19)	69.19 (477.05)
93.26 (642.99)	76.87 (530.03)	73.79 (508.74)	63.18 (435.63)
96.78 (667.26)	69.35 (478.14)	73.32 (505.54)	68.13 (469.75)
90.77 (625.81)	92.23 (635.90)	83.18 (573.51)	52.89 (364.68)
85.34 (588.39)	51.90 (357.86)	77.17 (532.04)	56.44 (389.12)
	74.45 (513.34)	82.95 (571.93)	68.28 (470.78)
	49.51 (341.37)	72.31 (498.56)	56.44 (389.12)
	70.79 (488.06)	73.32 (505.54)	56.30 (388.14)
	72.89 (502.54)	79.03 (544.90)	54.91 (378.62)
	84.97 (585.88)	75.44 (520.13)	65.03 (448.39)
	84.51 (582.66)		71.29 (491.51)
	88.98 (613.50)		63.67 (438.98)
	69.15 (476.80)		64.00 (441.24)
	74.24 (511.86)		65.48 (451.48)
	65.91 (454.41)		67.93 (468.36)
	66.32 (457.29)		67.65 (466.40)
	72.32 (498.66)		58.50 (403.37)
	67.06 (462.38)		56.80 (391.64)
	93.59 (645.28)		61.10 (421.28)
	94.65 (652.59)		50.24 (346.36)
	77.90 (537.07)		51.19 (352.95)
	89.55 (617.39)		69.16 (476.85)
	92.88 (640.39)		55.91 (385.47)
	88.88 (612.83)		58.98 (406.67)
	88.40 (609.48)		67.83 (467.69)
	69.80 (481.22)		56.19 (387.42)
	84.95 (585.68)		58.61 (404.09)
	84.11 (579.91)		58.99 (406.72)
	83.36 (578.17)		62.57 (431.42)
	80.54 (555.31)		
	83.75 (577.43)		
	79.92 (551.02)		
	72.01 (496.51)		
	82.55 (569.19)		
	77.96 (537.54)		
Mean	Mean	Mean	Mean
88.51 (610.23)	77.92 (537.21)	77.38 (533.51)	61.27 (422.46)
Standard Deviation	Standard Deviation	Standard Deviation	Standard Deviation
7.95 (54.82)	10.91 (75.23)	4.44 (30.62)	5.99 (41.31)

Table 9. Tension test results for extracted V2 type GFRP bars (#5 and #6)

V2 #5		V2 #6	
Tensile Strength No Exposure ksi (MPa)	Tensile Strength After Exposure ksi (MPa)	Tensile Strength No Exposure ksi (MPa)	Tensile Strength After Exposure ksi (MPa)
76.67 (528.62)	58.06 (400.31)	75.87 (523.12)	56.53 (389.76)
77.10 (531.56)	56.42 (388.98)	72.29 (498.42)	57.71 (404.82)
75.10 (517.79)	60.25 (415.40)	73.70 (508.15)	55.90 (385.43)
71.67 (494.17)	57.85 (398.87)	73.00 (503.31)	57.38 (395.64)
71.82 (495.15)	56.65 (390.61)	70.22 (484.15)	52.45 (361.61)
	54.85 (378.18)	73.94 (509.79)	58.26 (401.67)
	50.04 (344.99)	72.72 (501.41)	57.34 (395.36)
	52.83 (364.26)	73.32 (505.55)	57.23 (394.60)
	55.31 (381.37)	71.97 (496.22)	60.67 (418.28)
	52.94 (365.04)	71.46 (492.68)	52.90 (364.76)
	56.55 (389.89)		55.89 (385.33)
	56.62 (390.41)		53.30 (367.49)
	53.80 (370.96)		59.37 (409.34)
	54.93 (378.70)		57.47 (369.25)
	49.82 (343.50)		56.58 (390.09)
	54.73 (377.34)		61.80 (426.10)
	56.39 (388.79)		64.80 (446.76)
	54.46 (375.51)		
	54.78 (377.73)		
	55.95 (385.73)		
	52.87 (364.52)		
	56.76 (391.33)		
	53.32 (367.64)		
	53.03 (365.62)		
	51.97 (358.33)		
	55.90 (385.40)		
	56.34 (388.46)		
	54.18 (373.56)		
	55.38 (381.83)		
	56.95 (392.63)		
Mean	Mean	Mean	Mean
74.47 (513.46)	55.00 (379.20)	72.85 (502.28)	57.45 (396.08)
Standard Deviation	Standard Deviation	Standard Deviation	Standard Deviation
2.60 (17.91)	2.28 (15.72)	1.54 (10.59)	3.15 (21.71)

Table 10. Tension test results for extracted P type GFRP bars (#5 and #6)

P #5		P #6	
Tensile Strength No Exposure ksi (MPa)	Tensile Strength After Exposure ksi (MPa)	Tensile Strength No Exposure ksi (MPa)	Tensile Strength After Exposure ksi (MPa)
98.93 (682.07)	96.71 (666.78)	103.47 (713.41)	93.00 (641.20)
95.42 (657.86)	92.25 (636.06)	97.34 (671.17)	92.60 (638.48)
101.32 (698.60)	90.48 (623.83)	97.59 (672.83)	82.81 (570.95)
103.81 (715.71)	82.65 (569.89)	93.82 (646.88)	82.23 (566.93)
99.98 (689.36)	90.41 (623.38)	94.41 (650.90)	92.75 (639.46)
103.84 (715.97)	88.34 (609.06)	101.12 (697.21)	94.78 (653.47)
101.98 (703.15)	89.16 (614.72)	96.31 (664.03)	93.22 (642.71)
97.66 (673.35)	85.52 (589.67)	99.94 (689.07)	90.41 (623.35)
101.42 (699.25)	86.72 (597.93)	100.29 (691.48)	93.60 (645.37)
97.26 (670.55)	83.50 (575.74)	96.02 (662.02)	96.48 (665.18)
	73.91 (509.56)		85.82 (591.72)
	90.01 (620.58)		86.06 (593.33)
	89.28 (615.57)		87.52 (603.44)
	89.40 (616.41)		93.78 (646.58)
	81.78 (563.83)		86.71 (597.85)
			94.04 (648.39)
			96.62 (666.19)
			96.97 (668.55)
			92.61 (638.53)
			94.68 (652.76)
			87.95 (606.40)
			91.34 (629.73)
			87.46 (602.98)
			92.39 (636.97)
			88.08 (607.31)
			88.59 (610.78)
			92.08 (634.86)
			89.88 (619.73)
			90.17 (621.69)
			89.80 (619.17)
			91.09 (628.02)
			93.68 (645.87)
Mean	Mean	Mean	Mean
100.16 (690.59)	87.34 (602.20)	98.03 (675.90)	90.91 (626.81)
Standard Deviation	Standard Deviation	Standard Deviation	Standard Deviation
2.83 (19.48)	5.36 (36.96)	3.10 (21.37)	3.77 (26.03)

4.3. Modulus of Elasticity Tests

Data were gathered to assess the influence of time of embedment in concrete of the MOE at the GFRP bars. No significant changes in elastic modulus were observed between the control GFRP bars and GFRP bars embedded in concrete beams for 7 years. Statistical t-tests of equality at a 0.05 level of significance indicated that the hypothesis that the mean MOE for the GFRP bars embedded in concrete beams is the same as the mean MOE for the control bars cannot be rejected. That means there is no statistically significant evidence to conclude that the mean MOE of embedded GFRP bars differs from the mean MOE of control GFRP bars. This indicates that the MOE of GFRP bars is not reduced as a function of time up to 7 years. The comparison of modulus of elasticity between control and extracted bars as a function of concrete cover depth is shown in Fig. 12. APPENDIX B includes the MOE test data and the statistical t-tests for the control and exposed GFRP bars.

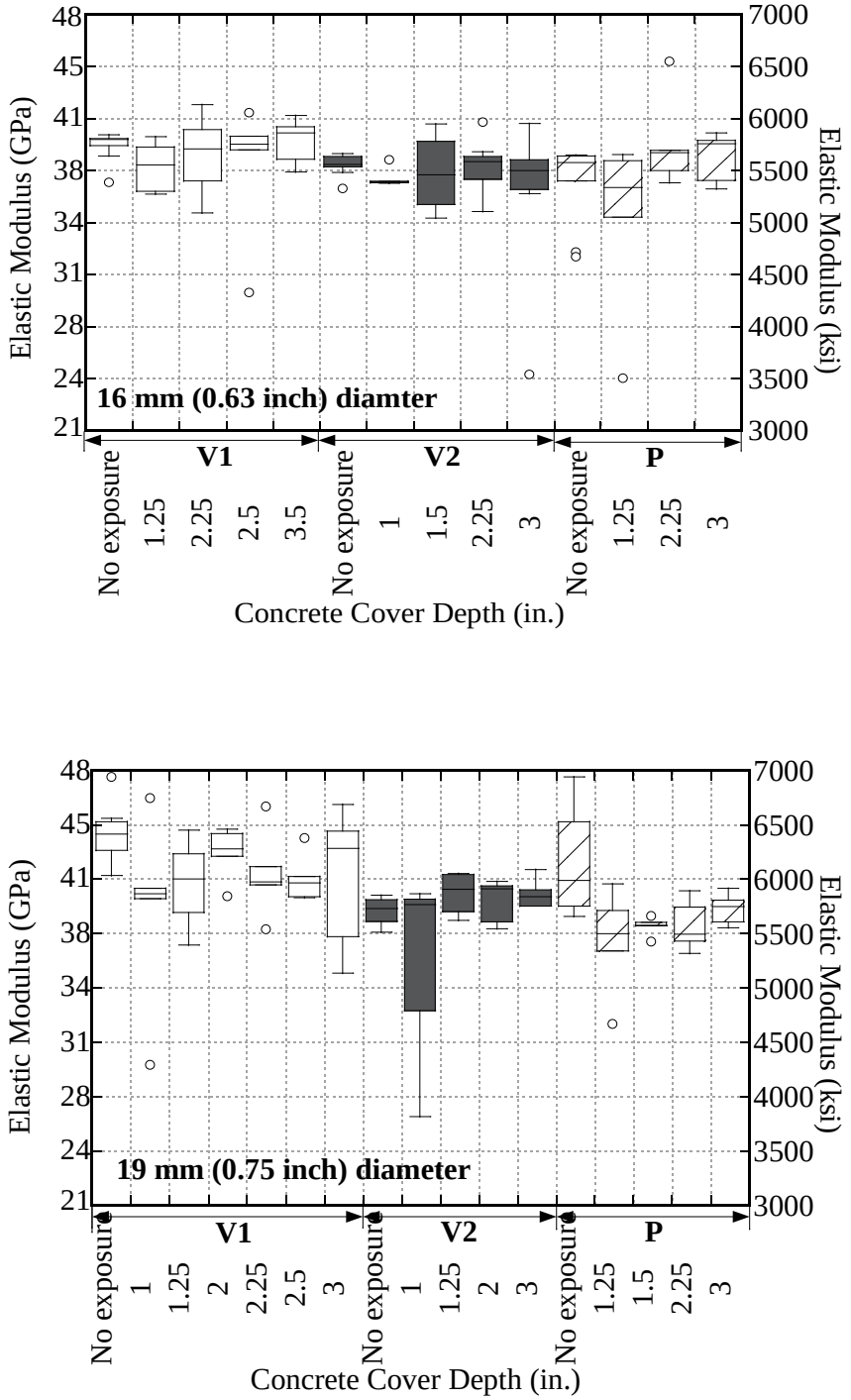

Fig. 12. Comparison MOE of GFRP bars (16 and 19 mm diameter)

4.4. GFRP Characterization Tests

SEM and EDX analysis were performed at the Microscopy Imaging Center (MIC) at Texas A&M University. These analyses focused on degradation of resin and the resin-fiber interface. The analysis did not identify deterioration at the glass fiber and polymer matrix interface. Fig. 13 through 15 shows the SEM micrographs and the EDX plots for the V1, V2, and P type GFRP bars, respectively. The EDX plots were obtained by scanning the resin spots (as shown in small pictures in EDX plots) in which alkalis might deteriorate. Table 11 exhibits changes in weight percent of silica and calcium contents; however, no significant difference between the exposed and control bars was observed in the EDX plots in Figs 13 through 15. The weight percent of silica and calcium in the exposed bars was less than in the control bars. Mukherjee and Arwikar (2005) reported that this is only possible if the molecular structure of fiber is changed when fibers have in contact with degenerating environmental solutions. These elements in concrete pore solution displace silica and calcium from the control bars.

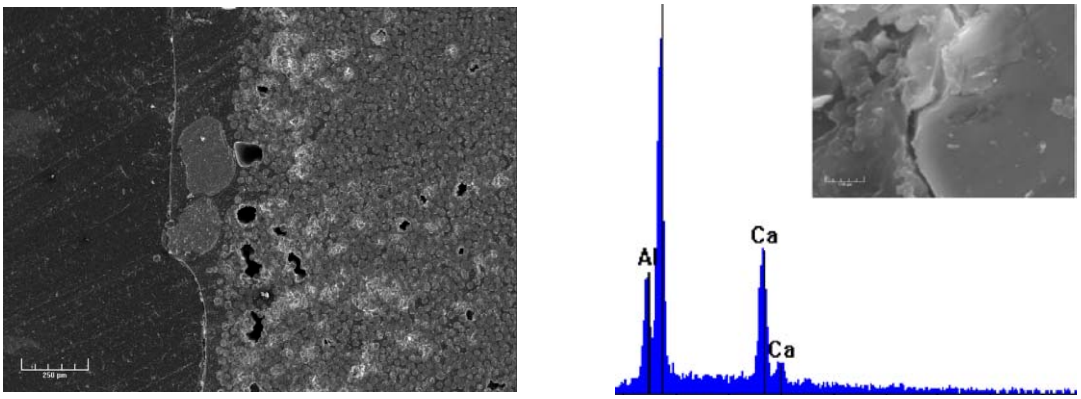

(a) V1 Control

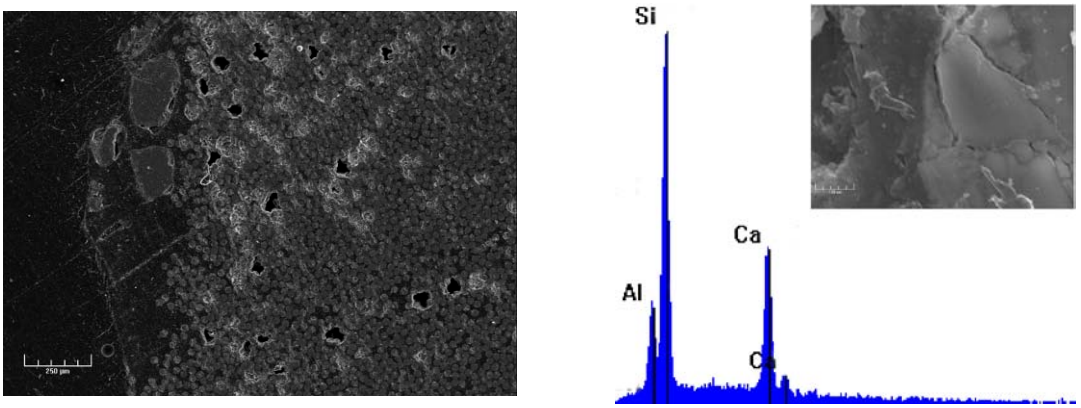

(b) V1 Exposed

Fig. 13. SEM and EDX of bar type V1

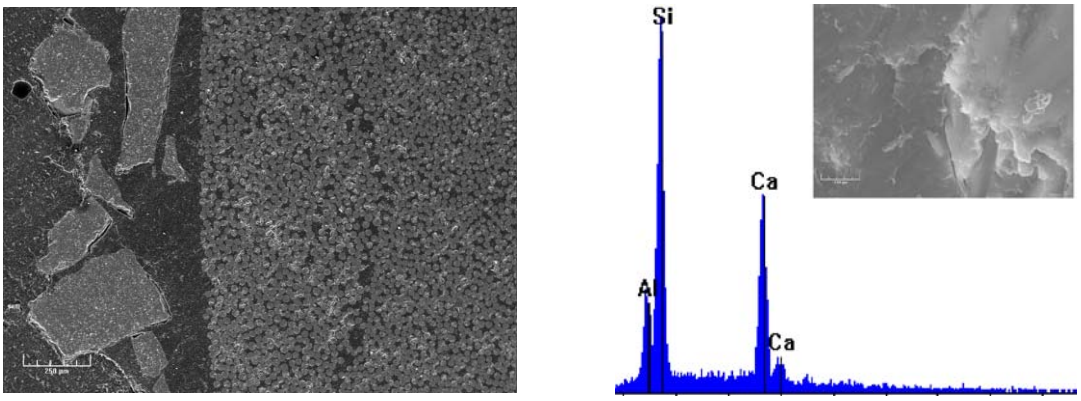

(a) V2 Control

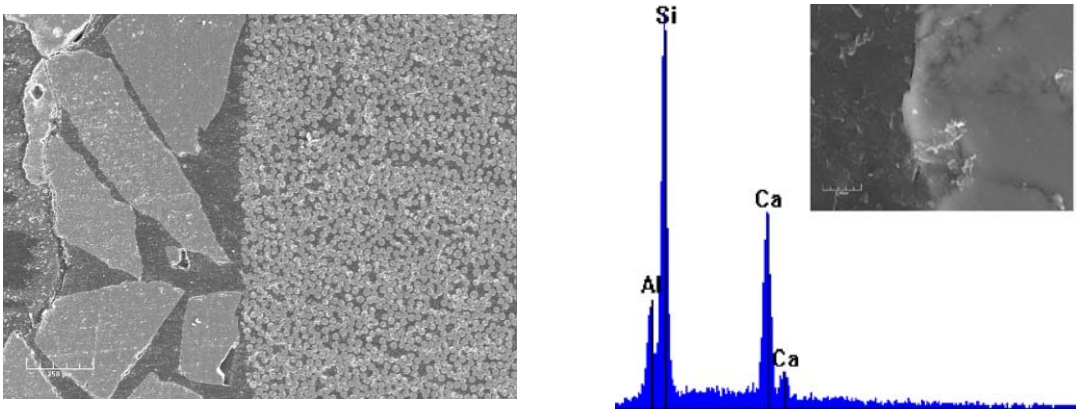

(b) V2 Exposed

Fig. 14. SEM and EDX of bar type V2

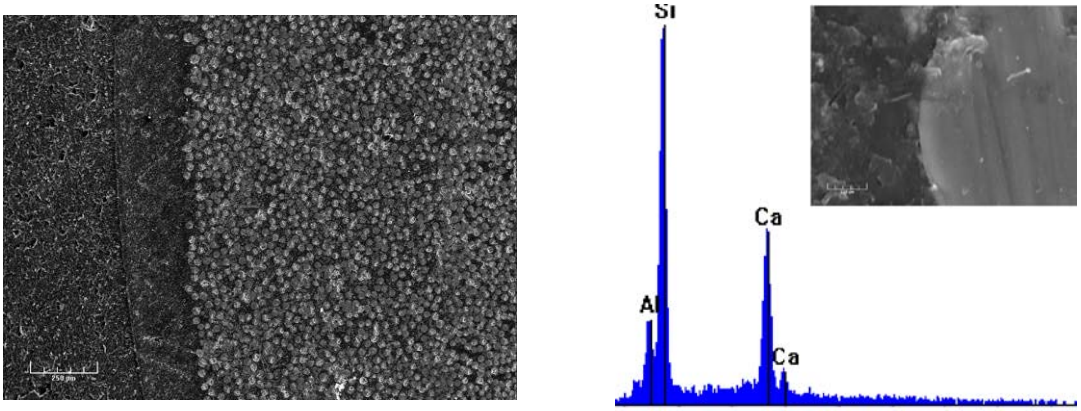

(a) P Control

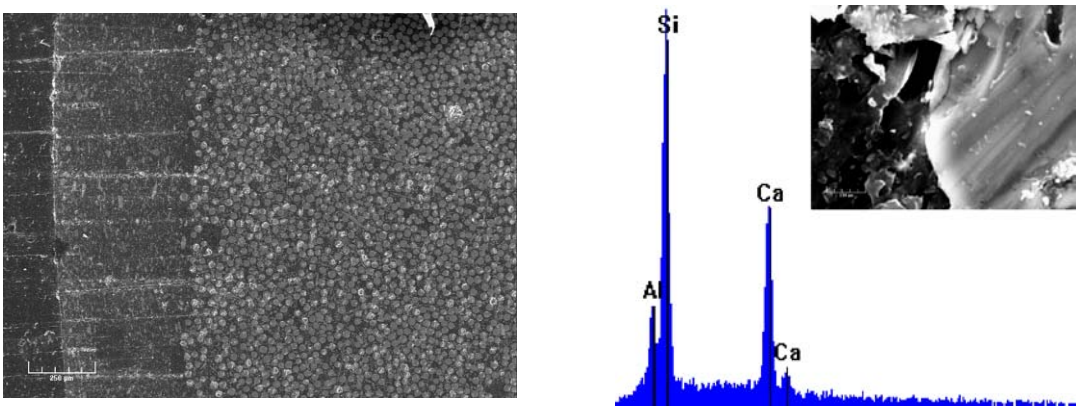

(b) P Exposed

Fig. 15. SEM and EDX of bar type P

Table 11. Energy Disperse X-ray (EDX) test results of each bar type

Element (wt %)	Si	Al	Ca
V1 control	8.26	2.62	6.04
V1 exposed	5.98	1.52	4.58
V2 control	9.06	2.32	8.11
V2 exposed	7.73	1.93	6.26
P control	9.95	2.14	7.30
P exposed	5.21	1.31	4.82

Figs. 16 through 18 show the results from FTIR tests. Changes in hydroxyl group and carbon-hydrogen (C-H) group were detected.

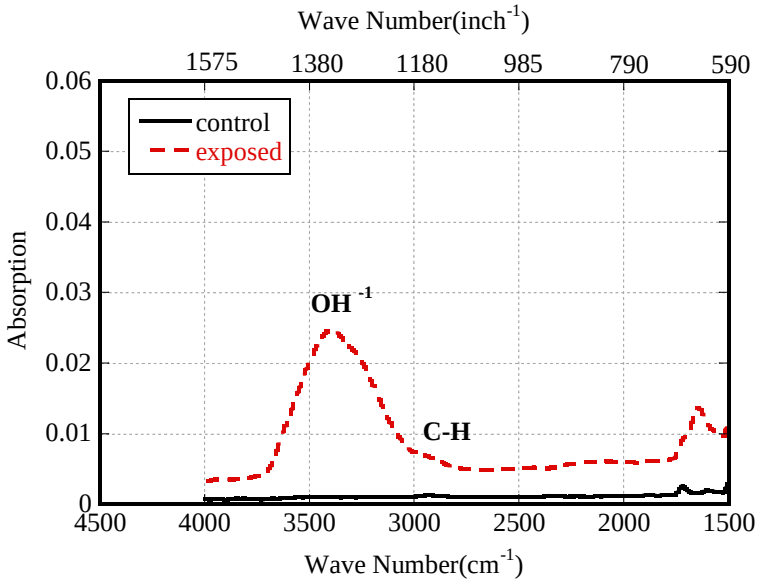

Fig. 16. FTIR results for exposed and control bar type V1

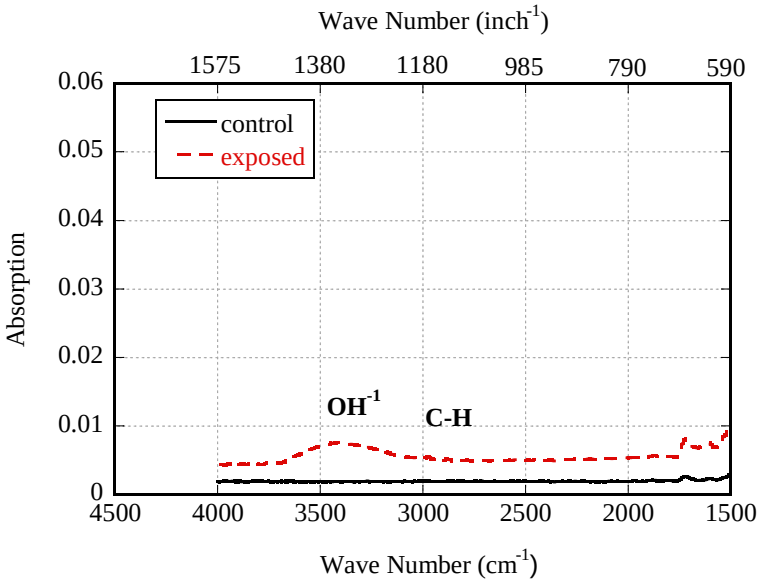

Fig. 17. FTIR results for exposed and control bar type V2

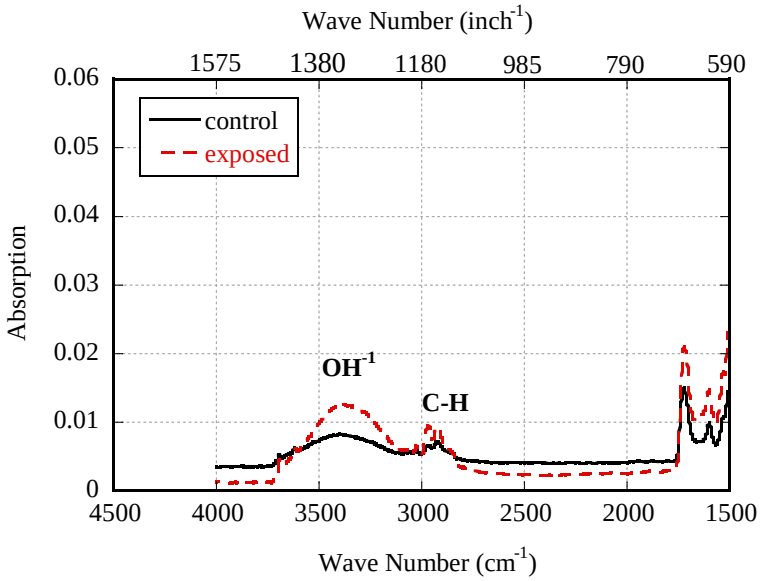

Fig. 18. FTIR results for exposed and control bar type P

From test results of FTIR, changes in relative amount of absorption band corresponding to the hydroxyl group (at wave-number of 3400 cm^{-1}) and to the C-H group (at wave-number of 2900 cm^{-1}) between the control (solid line) and the exposed GFRP bars (dotted line) was detected in this analysis. For all types exposed GFRP bars, the relative absorption amount of hydroxyl group exhibits higher values in all bar types and changes in C-H groups were observed in type P bars. It might be reported that alkalis in concrete induced in polymer matrix and broke the ester resin chain and the hydrolysis reaction occurred when the GFRP bars were embedded in concrete.

In DSC test results, it was reported that when moisture and solutions induces and breaks the polymer chains, the glass transition temperature is reduced through plasticization. Changes in glass transition temperature (T_g) are caused by moisture or

alkali attack. In this analysis, there is almost no difference in glass transition temperature of polymer matrix of between control and exposed GFRP reinforcement. Robert et al. (2009) reported that the T_g of polymer resin of the exposed and of the same control GFRP bars could be in the range in DSC tests due to the reversible plasticizing caused by moisture absorption. In terms of the test results, the changes in the range of T_g were negligible and it could be expected due to the reversible plasticization. Antoon and Koenig (1980) reported that the changes in mechanical properties of composite materials exposed to moisture may be reversible, partially reversible, irreversible, or combination of these types depending on exposure time and conditions. For reversible process that involves plasticization and swelling of the resin matrix, mechanical properties usually be stored by drying. Figs. 19 through 21 show DSC test results of each bar type GFRP bars, V1, V2, and P, respectively.

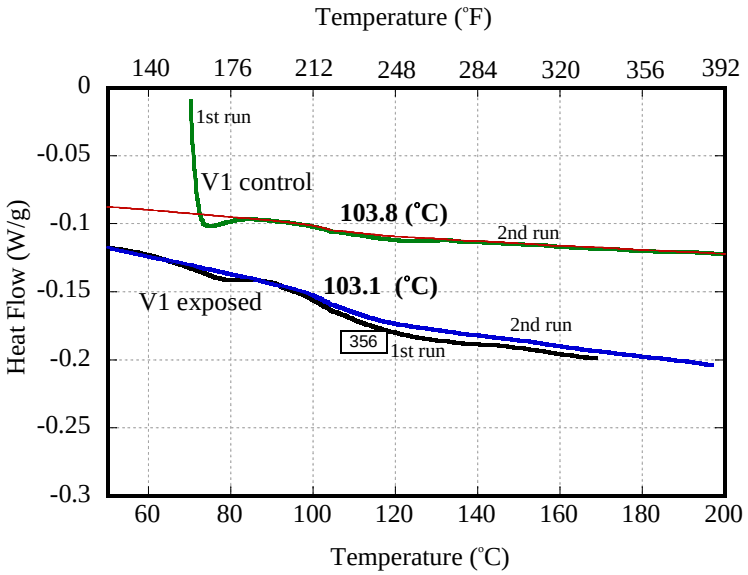

Fig. 19. DSC results for bar type V1

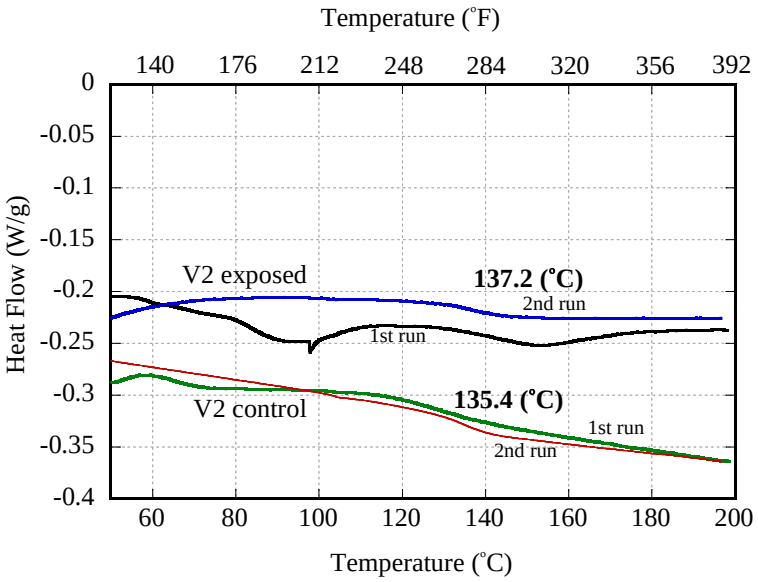

Fig. 20. DSC results for bar type V2

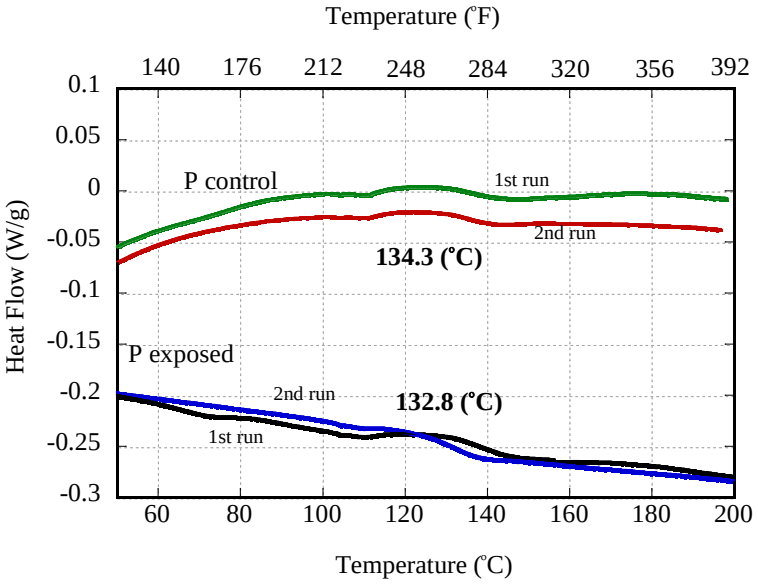

Fig. 21. DSC results for bar type P

Because the glass fibers are significantly responsible for mechanical properties, AASHTO (2008) describes the permitted constituent materials and limits on constituent volumes and performance requirements for GFRP bars in concrete. When ASTM D 2584 (Standard Test Method for Ignition Loss of Cured Reinforced Resins, 2008) is used, the glass fiber volume contents shall not be less than 70 percent by weight. Trejo et al. (2005) reported that all bar type V1, V2, and P contained approximately contained 70 percent the glass fibers volume and 30 percent resin matrix. The TGA test results indicated that the significant weight loss of polymer resin from 300 °C (572 °F) to 450 °C (842 °F) and the approximate left behind glass fiber contents of the #5 (16 mm, 0.63 inch) diameter of the type V1, V2, and P bars were 82, 77, and 67 percent, respectively. The type P bar (#5) does not meet the required 70 percent minimum glass fiber contents. Test results from the TGA tests as shown in Figs. 22 and 23.

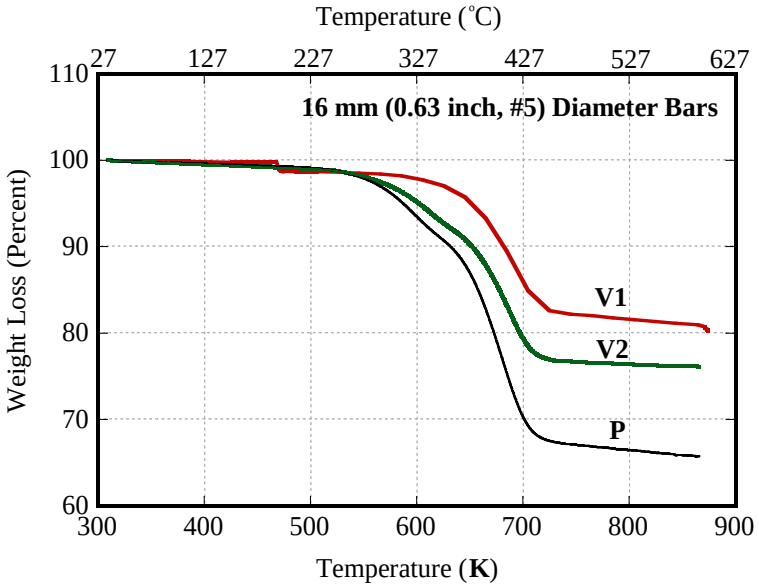

Fig. 22. TGA results of 16 mm (0.63 inch) diameter GFRP bars

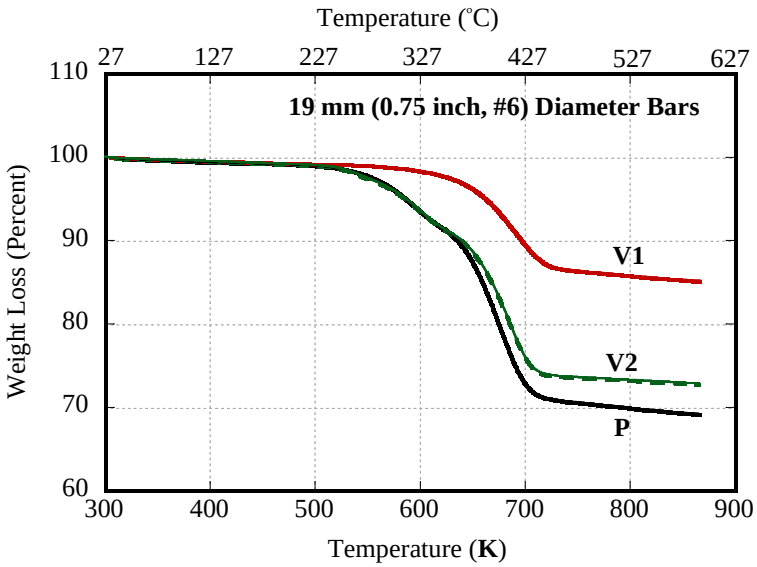

Fig. 23. TGA results of 19 mm (0.75 inch) diameter GFRP bars

4.5. Concrete Characterization Tests

The pH values for all concrete pore solution evaluated in this research varied from 12.25 to 13.05, which is typical of un-carbonated field concrete. Furthermore, these values are representative of the values used in many accelerated aging tests in literature. The range of pH values of the concrete pore solution is shown in Fig. 24. The pH tests were performed with three samples for each concrete beam and the test results were referred as pH 1, 2 and 3 in Fig. 24. The volume of the permeable voids in the concrete ranged from 11.5 to 17.1 percent, and average across all beams is 13.85 percent. The test results from the void and absorption tests are plotted as shown in Fig. 25. Two samples per each beam were extracted and tested as sample 1 and 2 in Fig. 25. Based on the concrete

characterization tests of alkalinity and permeable voids, no significant difference were identified between different GFRP bars types and concrete beams.

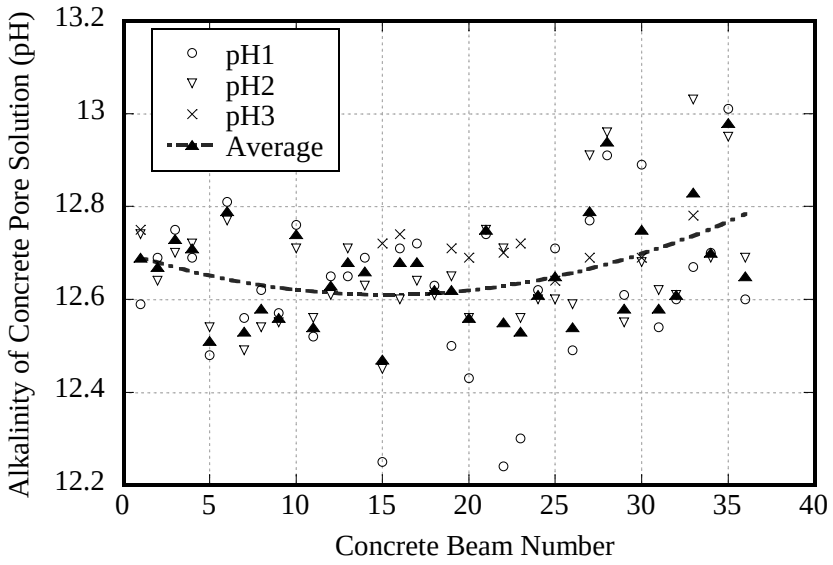

Fig. 24. Alkalinity of concrete pore solution

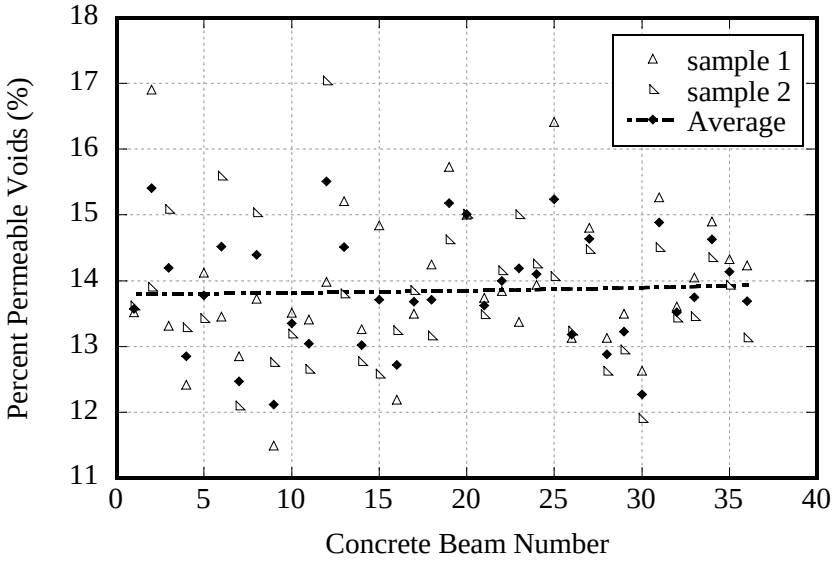

Fig. 25. Void, density, and absorption of concrete

4.6. Analysis of Potential Influencing Factors

Fig 26 exhibits the concrete beam storage position for 7 years exposure. It was hypothesized that the beams stacked at top position were likely exposed to higher temperature and moisture condition than the beams stacked below the top position. To assess if the beam storage position affected on the capacity of embedded GFRP bars, tensile capacity of GFRP bars embedded in top beams was compared to the tensile capacity of GFRP bars embedded in the beams below the top position. It is noted that because none of the top beams was embedded with type P bars, there were not assessed. The statistical t-tests of equality at 0.05 level of significance indicated that the hypothesis that the mean tensile capacity for the GFRP bars embedded in the top beams is the same as the mean tensile capacity for the GFRP bars embedded in the beams below the top cannot be rejected. That means there is no statistically significance evidence to conclude that beam storage position results in a different mean capacity of the GFRP bars embedded in concrete beams. Fig 27 shows a box plot of the GFRP bar capacities from the top beams and the beams below the top.

Fig. 26. Storage positions of GFRP reinforced beams

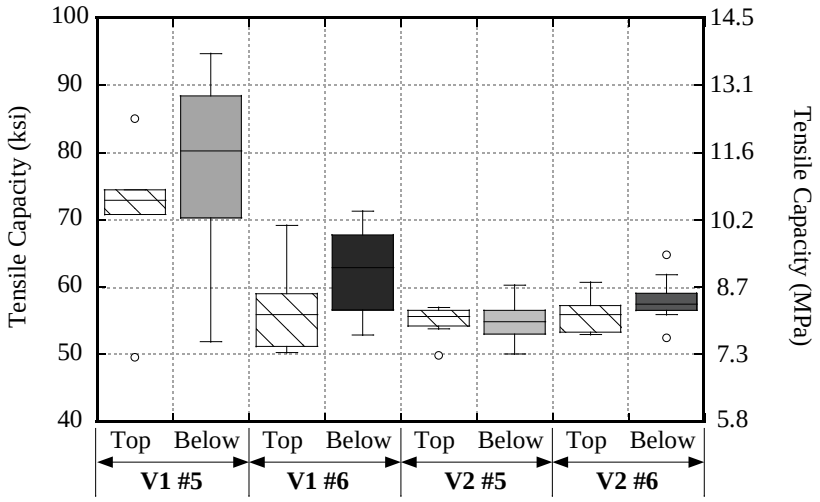

Fig. 27. Comparison of Capacity of GFRP bars stored at different locations

To analyze the effects of the material factors, the tensile strength of GFRP bars was normalized and plotted as a function of the alkalinity of concrete pore solution, percent porosity, and concrete cover depth. Because the tensile strength could be affected by these characteristics, these may have to be considered and included as a design parameter in a newly developed prediction model. However, as shown in Figs. 28 through 30, there were no outstanding influencing potential factors for all material characteristic evaluated in this research. Fig 26 represents the alkalinity of concrete pore solutions varied approximately 12.5 to 13 and this variation is almost consistent. If the range of alkalinity of pore solution in concrete beams were larger, the effect of pH values on tensile capacity on the embedded GFRP bars could be recognized.

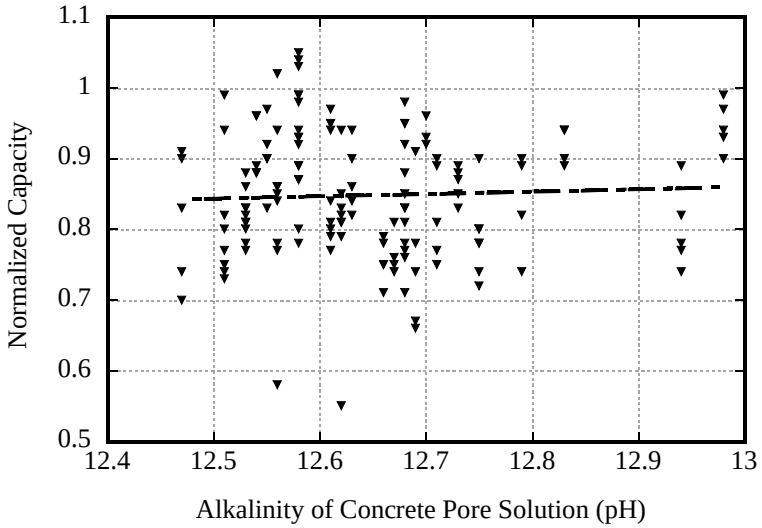

Fig. 28. Normalized capacity as a function of alkalinity (pH)

The amount of moisture and pore solution can be determined by the quantity of the permeable voids and porosity in concrete material. Although the Fig. 29 shows a somewhat positive slope, the porosity variation evaluated in this research had no significant effect on the capacity of the extracted GFRP reinforcing bars. Because the moisture contents can varies as different cover depth of concrete, the normalized capacity was plotted as a function of cover depth as shown in Fig. 30. The influence of cover depth on tensile capacity is not significant.

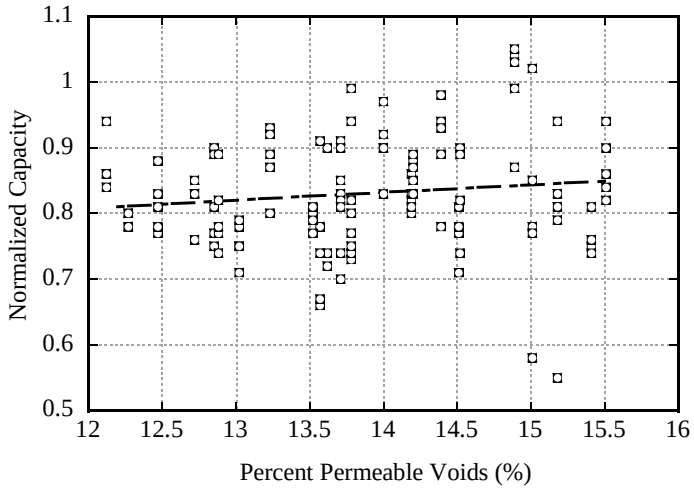

Fig. 29. Normalized capacity as a function of porosity

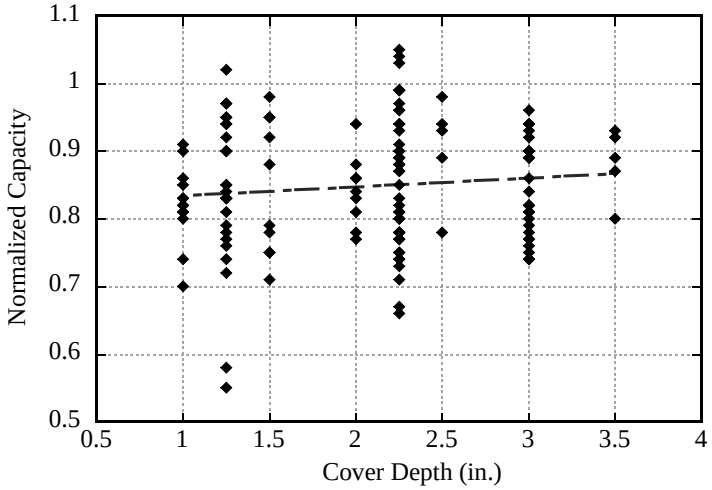

Fig. 30. Normalized capacity as a function of cover depth

5. TIME VARIANT PROBABILISTIC CAPACITY MODEL FOR GFRP BARS

This section describes methodologies to construct a probabilistic capacity model. In addition to measured data of 16 and 19 mm (0.63 and 0.75 inches or, named #5 and #6, respectively), limited experimental data available from literature on GFRP reinforcement with average 9 mm (0.35 inch or, named #3 bars) diameter was used when the probabilistic capacity model was developed. Based on the observational outcomes, likelihood function and Bayesian updating were used to assess unknown parameters. The developed time-variant model is a probabilistic capacity model to properly account for the statistical uncertainties, considering the influence of the missing variables and remaining error due to the inexact model form (Gardoni et al. 2002). This developed time-variant probabilistic model provides the required information to assess the safety and performance of GFRP reinforcing bars and of concrete structures reinforced with these materials.

5.1. Formulation of Probabilistic Capacity Model for GFRP Bars

The prediction model suggested by Trejo et al. (2005) was firstly modified to fit the experimental outcomes. A prediction model is constructed using an existing diffusion model form as follows:

$$\sigma_t = \left[1 - \lambda\left(\frac{D \cdot t}{R_0^2}\right)^{\alpha}\right]\mu_{\sigma_0} \tag{10}$$

where σ_t is tensile strength at time t, λ is strength reduction factor, D is diffusion coefficient, t is exposure time, R_0 is bar radius at $t = 0$, α is power for nonlinear function, and μ_{σ_0} is the mean of tensile strength of bars before exposure and is average values of each bar type and each bar diameter. The test results and normalized tensile capacity value, $\sigma_t / \mu_{\sigma_0}$, of each bar type and diameter were provided in APPENDIX A.

To account for the relevant sources of uncertainties, including the statistical uncertainty in the assessment of the unknown parameters and considering the influence of the missing variables and remaining model error due to the inexact model form, Error term, $s_0 \cdot \varepsilon_0$ and $s \cdot \varepsilon$ are added to Equation (10) and then modified as follows:

$$\frac{\sigma_t(\mathbf{x}, \boldsymbol{\Theta})}{\mu_{\sigma_0}} = \left[(1 + s_0 \cdot \varepsilon_0) - \lambda \left(\frac{D \cdot t}{R_0^2} \right)^{\alpha} (1 + s \cdot \varepsilon) \right] \tag{11}$$

where $\mathbf{x} = (D, R_0)$ is the vector of basic variables, $\boldsymbol{\Theta} = (\lambda, \alpha, s_0, s)$ is a vector of unknown model parameters introduced to fit the experimental data. Likelihood function and Bayesian approach were used to estimate the statistics (means, covariance, and correlation coefficients) of the unknown parameters. Error terms of $s_0 \cdot \varepsilon_0$ and $s \cdot \varepsilon$ are added to capture the variability of σ_0 around its mean μ_{σ_0} and of the reduction terms, $\lambda (D \cdot t / R_0^2)^{\alpha}$, respectively. ε_0 and ε are statistically independent normally distributed random variables with zero means and unit variance (normality assumption), and the coefficient s_0 and s are the constant standard deviation of the two error terms (homoskedasticity assumptions).

5.2. Bayesian Parameter Estimation

The unknown parameters $\boldsymbol{\Theta}$ are estimated by use of the Bayesian updating rules (Box and Tiao 1992)

$$f(\boldsymbol{\Theta}) = \kappa L(\boldsymbol{\Theta})\, p(\boldsymbol{\Theta}) \tag{12}$$

where $\kappa = [\int L(\boldsymbol{\Theta})\, p(\boldsymbol{\Theta}) d(\boldsymbol{\Theta})]^{-1}$ is a normalizing factor. $f(\boldsymbol{\Theta})$ is posterior distribution of $\boldsymbol{\Theta}$ determined using Bayesian rule in Equation (12) by representing our updated state of knowledge about $\boldsymbol{\Theta}$; $p(\boldsymbol{\Theta})$ is prior distribution reflecting our state of knowledge about $\boldsymbol{\Theta}$ prior to obtaining the observations, that means the tensile strength data, $\mathbf{D}$, from total number of GFRP reinforcing bar specimens, n. In this analysis, a non-informative prior distribution provided in Box and Tiao (1992) was used to assume that there is no information available about the model parameters before the experimental outcomes. $L(\boldsymbol{\Theta})$ is the likelihood function that represents the information on the model parameters, $\boldsymbol{\Theta}$, from a set of tensile strength data, $\mathbf{D}$, and is proportional to the conditional probability, $p(\mathbf{D}|\boldsymbol{\Theta})$, of observing experimental outcomes, $\mathbf{D}$ for given values of $\boldsymbol{\Theta}$. To formulate the likelihood function, Equation (11) can be written as:

$$\frac{\sigma_t(\mathbf{x},\boldsymbol{\Theta})}{\mu_{\sigma_0}} = \left[1 - \lambda\left(\frac{D\cdot t}{R_0^2}\right)^{\alpha}\right] + \left\{s_0 \cdot \varepsilon_0 - \lambda\left(\frac{D\cdot t}{R_0^2}\right)^{\alpha} s\cdot\varepsilon\right\} \tag{13}$$

and, because ε_0 and ε are assumed to have a normal distribution (normality assumption) and uncorrelated, Equation (13) can be modified as:

$$\frac{\sigma_t(\mathbf{x},\boldsymbol{\Theta})}{\mu_{\sigma_0}} = \left[1 - \lambda\left(\frac{D\cdot t}{R_0^2}\right)^{\alpha}\right] + \sqrt{s_0^2 + \lambda^2\left(\frac{D\cdot t}{R_0^2}\right)^{2\alpha} s^2\varepsilon} \tag{14}$$

For $i-$th data point in total number of experimental data, n, the residual tensile strength, $r_i(\lambda,\alpha)$, was obtained by subtracting the mean strength value in Equation (14) from the actual strength measured in the field as follows:

$$r_i\left(\lambda,\alpha\right)=\frac{\sigma_{ti}}{\mu_{\sigma_{0i}}}-\left[1-\lambda\left(\frac{D\cdot t_i}{R_{0i}^2}\right)^{\alpha}\right] \tag{15}$$

Under the assumptions of statistically independent observations, the likelihood function, $L(\boldsymbol{\Theta})$, can be written as the product of the probability of observing each residual tensile strength, $r_i(\lambda,\alpha)$:

$$L\left(\boldsymbol{\Theta}\right)=\prod_{i=1}^{n} p\left[\sqrt{s_0^2+\lambda^2\left(\frac{D\cdot t_i}{R_{0i}^2}\right)^{2\alpha}s^2}\,\varepsilon_i=r_i\left(\lambda,\alpha\right)\right] \tag{16}$$

since ε has the standard normal distribution, $L(\boldsymbol{\Theta})$ can be written as:

$$=\prod_{i=1}^{n}\left\{\frac{1}{\sqrt{s_0^2+\lambda^2\left(\frac{D\cdot t_i}{R_{0i}^2}\right)^{2\alpha}s^2}}\varphi\left[\frac{r_i\left(\lambda,\alpha\right)}{\sqrt{s_0^2+\lambda^2\left(\frac{D\cdot t_i}{R_{0i}^2}\right)^{2\alpha}s^2}}\right]\right\} \tag{17}$$

where $\varphi(\cdot)$ denotes the standard normal probability density function (PDF).

Table 12 lists the updated posterior statistics of parameters.

Table 12. Updated posterior statistics of the parameters

Parameter	Mean	Standard Deviation	Correlation Coefficient			
			λ	α	σ_0	σ
λ	0.135	0.011	1			
α	0.207	0.082	– 0.84	1		
σ_0	0.039	0.003	–0.04	0.04	1	
σ	0.557	0.043	–0.28	–0.02	–0.25	1

In terms of Bayesian updating, Figs. 31 through 33 exhibit comparison of deterioration rate between the predicted and normalized measured tensile capacity, $\sigma_t / \mu_{\sigma_0}$,as a function of time. The circles (◦) show experimental data for all GFRP bar types, and the solid lines presents the prediction of mean normalized stress capacity (in the top plot for #3 bars, in the mid plot for #5 bars, and in the bottom plot for the #6 bars, respectively). The dotted curves show the region with one standard deviation of the mean. The horizontal dashed-dotted lines represent ACI 440 and the AASHTO (2008) design strength considering environment reduction factor over time. The smaller diameter bars show faster deterioration in capacity than lager bars. It was also observed that the mean prediction of normalized capacity shows fast decrease in first few years, and gradually slows down as time increase.

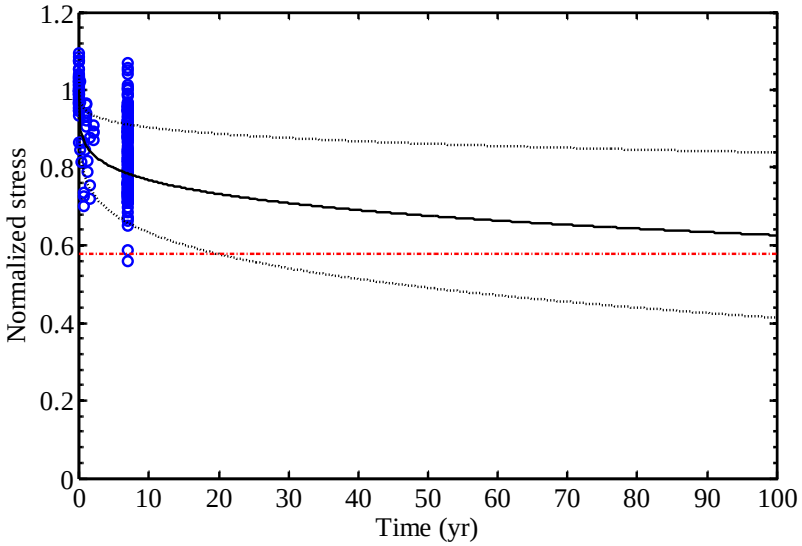

Fig. 31. Deterioration of 9 mm (0.35 inch) GFRP bars

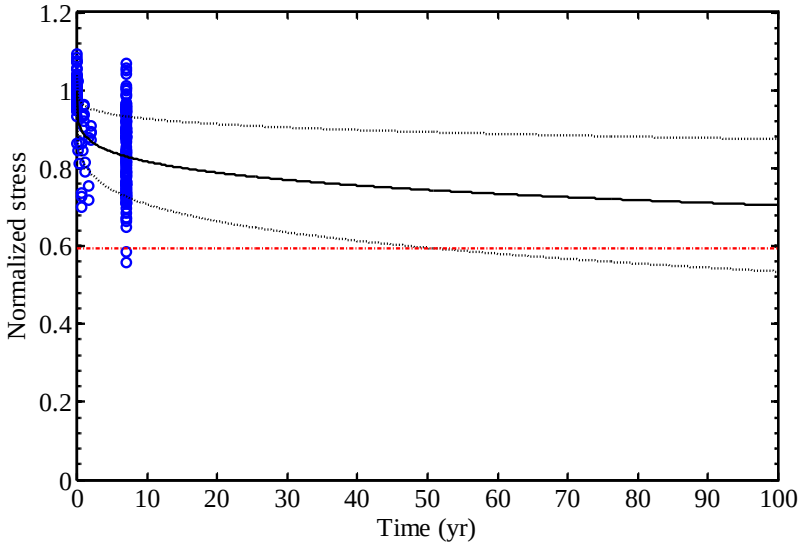

Fig. 32. Deterioration of 16 mm (0.63 inch) GFRP bars

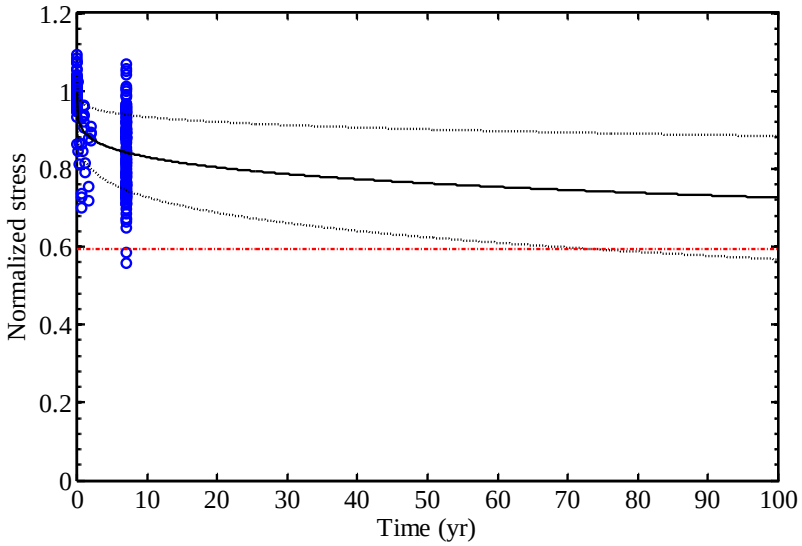

Fig. 33. Deterioration of 19 mm (0.75 inch) GFRP bars

5.3. Limit State Function

A limit state function $g(\cdot)$ was introduced such that the event $\{g(\cdot) \le 0\}$ denotes not meeting a specified capacity requirement. In this analysis, the ACI 440 and AASHTO design strength was used as a specified capacity requirement. Using a developed time-variant probabilistic model, the limit state function can be defined as:

$$g_t(\mathbf{x}, \boldsymbol{\Theta}) = C_t(\mathbf{x}, \boldsymbol{\Theta}) - C_{aci}(\mathbf{x}) \tag{18}$$

where $C_{aci}(\mathbf{x})$ = design strength by ACI 440 and AASHTO Specifications considering environment reduction factor, and $C_t(\mathbf{x}, \boldsymbol{\Theta})$ = updated capacity model. In the capacity model, $\mathbf{x}$ is the vector of measurable variables, and $\boldsymbol{\Theta}$ is the vector of unknown parameters.

The probabilistic capacity model in Equation (14) with observational data can be rewritten as:

$$C_t(\mathbf{x},\boldsymbol{\Theta}) = \left[1-\lambda\left(\frac{D\cdot t}{R_0^2}\right)^{\alpha}\right] + \sqrt{s_0^2+\lambda^2\left(\frac{D\cdot t}{R_0^2}\right)^{2\alpha} s^2\varepsilon} \tag{19}$$

where $\boldsymbol{\Theta} = (\lambda, \alpha, s_0, s)$ are model parameters assessed in terms of experimental data from the concrete beams. ε_0 and ε are the errors that have normal distribution with zero mean and unit standard deviation. The normalized design strength issued by ACI 440 and AASHTO, $C_{aci}(\mathbf{x})$, can be written as:

$$C_{aci}(\mathbf{x}) = \frac{C_E f_{fu}^*}{\mu_{\sigma_0}} = \frac{f_{fu}}{\mu_{\sigma_0}} \tag{20}$$

where f_{fu} is a tensile strength considering the strength reduction factor, C_E, and normalized by initial values of unexposed GFRP bars to be consistent with the dimensionless of capacity model in the limit state function. Using Equation (19) and (21), the limit state function can be expressed as:

$$g_t(\mathbf{x},\boldsymbol{\Theta}) = \left\{\left[1-\lambda\left(\frac{D\cdot t}{R_0^2}\right)^{\alpha}\right] + \sqrt{s_0{}^2+\lambda^2\left(\frac{D\cdot t}{R_0^2}\right)^{2\alpha} s^2\varepsilon}\right\} - \frac{C_E f_{fu}^*}{\mu_{\sigma_0}} \tag{21}$$

Table 13 and Table 14 describe the distribution of random variables and the correlation coefficient of random variables for limit state function, respectively.

Table 13. Distribution of random variables

Random Variables	Bar size	Distribution	Mean	Standard Deviation	Reference
	#3	Lognormal	0.824	0.06	-
f_{f_u} (normalized)	#5	Lognormal	0.850	0.06	-
	#6	Lognormal	0.850	0.04	-
D (m^2/sec)		Lognormal	8.9E-13	3.5E-13	Trejo et al. (2005)
	#3	Lognormal	4.5	0.55	Kulkarni, S. (2006)
R (mm)	#5	Lognormal	8	0.97	Kulkarni, S. (2006)
	#6	Lognormal	19	1.17	Kulkarni, S. (2006)
λ		Lognormal	0.135	0.011	posterior
α		Lognormal	0.207	0.082	posterior
s_0		Lognormal	0.039	0.003	posterior
s		Lognormal	0.557	0.043	posterior
ε		Normal	0	1	-
ε_0		Normal	0	1	-

Standard deviation of R (bar radius): C.O.V= 1.5 % (previous research by Kulkarni, S. 2006)

Table 14. Correlation coefficient of random variables

	f_{f_u}	D	R	λ	α	s_0	s	ε	ε_0
f_{f_u}	1								
D	0	1							
R	0	0	1						
λ	0	0	0	1					
α	0	0	0	–0.84	1				
s_0	0	0	0	–0.04	0.04	1			
s	0	0	0	–0.28	–0.02	–0.25	1		
ε	0	0	0	0	0	0	0	1	
ε_0	0	0	0	0	0	0	0	0	1

5.4. Sensitivity Analysis

Sensitivity and importance analysis could be computed using the reliability software, FERUM. In assessing reliability, sensitivity analysis is carried out to investigate which parameter is the most sensitive to the deterioration of the tensile capacity of the GFRP bars. Assuming $\mathbf{x}$ is the vector of random variables, let $f(\mathbf{x},\boldsymbol{\Theta}_f)$ be the probability density function of the random variables in $\mathbf{x}$, where $\boldsymbol{\Theta}_f$ is a set of distribution parameters defining the distribution of random variable such as means, standard deviations, correlation coefficient and other parameters. In this application, the posterior mean values obtained by Bayesian updating are considered as the parameters for the sensitivity analysis. The sensitivity measure for each parameter in given by computing the gradient of the reliability index, β, with respect to each parameter. Following Hohenbichler and Rackwitz (1983), the sensitivity of β to each parameter of interest in $\boldsymbol{\Theta}_f$ is given as:

$$\nabla_{\boldsymbol{\Theta}_f}\beta = \boldsymbol{\alpha}^{\mathrm{T}} \cdot \mathrm{J}_{\mathbf{u}^*,\boldsymbol{\Theta}_f} \tag{22}$$

where $\mathrm{J}_{\mathbf{u}^*,\boldsymbol{\Theta}_f}$ is the Jacobian of the probability transformation from the original space $\mathbf{x}$ to the standard normal space $\mathbf{u}$ with respect to the parameters $\boldsymbol{\Theta}_f$ and computed at the most likely failure point (design point), $\mathbf{u}^*$, and the vector $\boldsymbol{\alpha}$ is defined as:

$$\boldsymbol{\alpha} = \frac{\nabla G}{\|\nabla G\|}, \nabla G = \left\{ \frac{\partial G}{\partial u_1}, \frac{\partial G}{\partial u_2}, ..., \frac{\partial G}{\partial u_k} \right\}^{\mathrm{T}} \tag{23}$$

where $\nabla(\cdot)$ is the gradient function, G is the limit state function and k is total number of random variables. In order to compare the sensitivity measures of all parameters, we define the vector, $\boldsymbol{\delta}$, as follows:

$$\boldsymbol{\delta} = \boldsymbol{\sigma} \cdot \nabla_{\boldsymbol{\Theta}_f} \beta \tag{24}$$

where $\boldsymbol{\sigma}$ is a diagonal matrix with diagonal elements given by standard deviation of each random variable in $\mathbf{x}$. By multiplying the sensitivity vector, $\nabla_{\boldsymbol{\Theta}_f} \beta$ with the standard deviation matrix, $\boldsymbol{\sigma}$, each term in $\boldsymbol{\delta}$ can be dimensionless and makes the parameter variations proportional to the corresponding standard deviations, which are measures of the underlying uncertainties.

Figs. 34 through 36 present the sensitivity of each bar diameter over time. Although the component of $\nabla_{\boldsymbol{\Theta}_f} \beta$ have different unit, and thus cannot be used to determine the ranking of parameters, it is valuable to plot the sensitivity analysis to changes in various parameters over time.

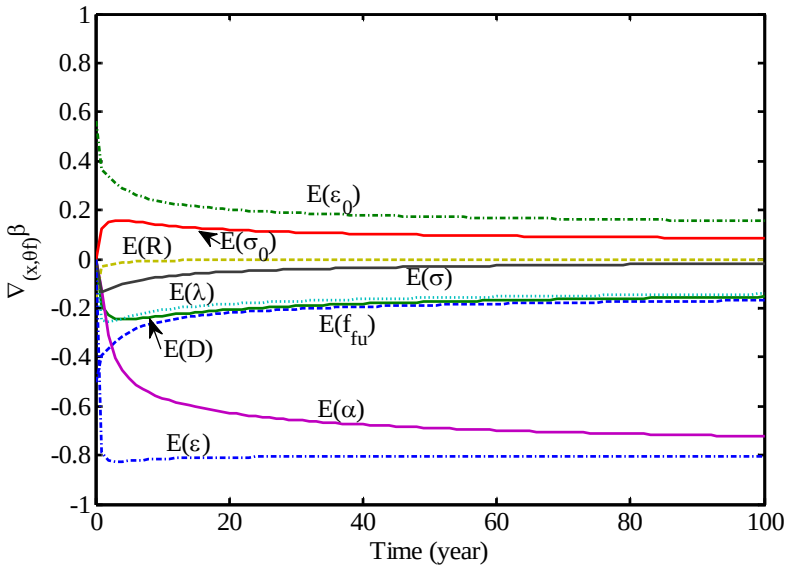

Fig. 34. Sensitivity analysis of 9 mm (0.35 inch) GFRP bars

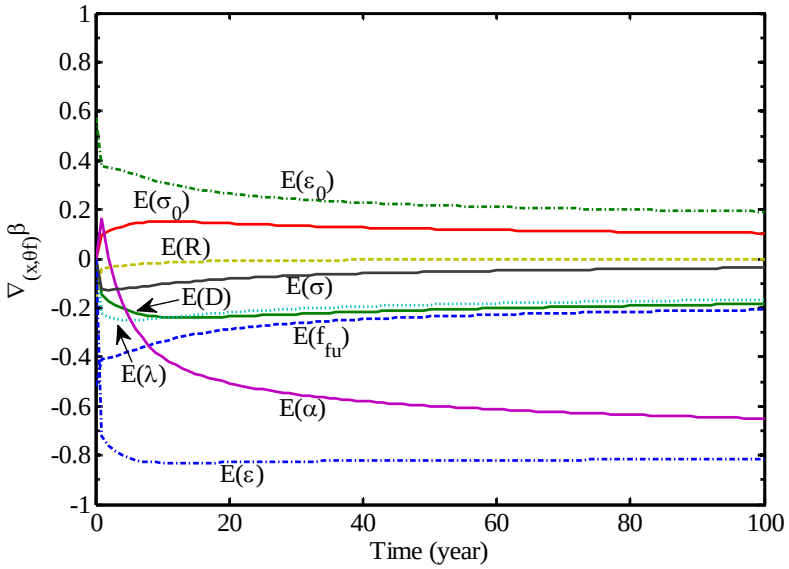

Fig. 35. Sensitivity analysis of 16 mm (0.63 inch) GFRP bars

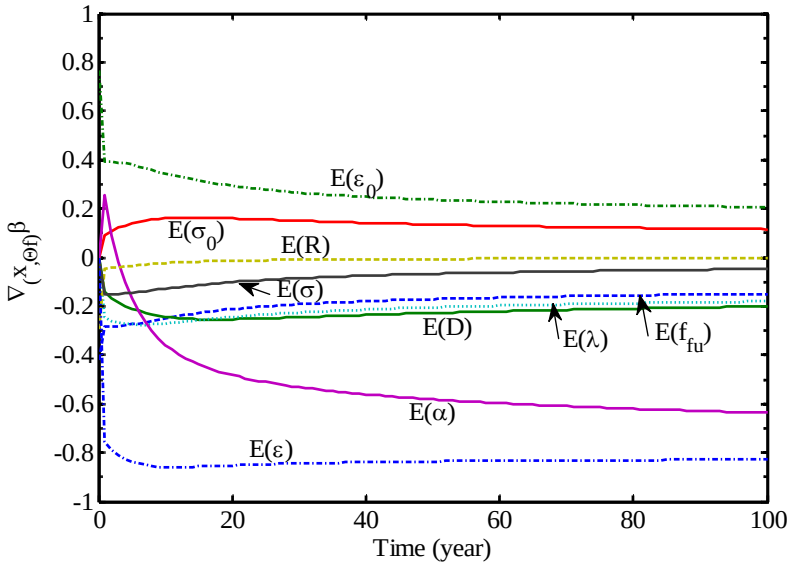

Fig. 36. Sensitivity analysis of 19 mm (0.75 inch) GFRP bars

5.5. Importance Analysis

In the limit state function, the influence of each random variable on the variance of the limit state function is different. In other words, each random variable has different contribution to the variability of the limit state function. Following Kiureghian and Ke (1985), the measure of importance is defined as:

$$\boldsymbol{\gamma}^{\mathbf{T}} = \frac{\boldsymbol{\alpha}^{\mathbf{T}} \mathbf{J}_{\mathbf{u}^*,\mathbf{z}^*} \mathbf{SD}'}{\left\| \boldsymbol{\alpha}^{\mathbf{T}} \mathbf{J}_{\mathbf{u}^*,\mathbf{z}^*} \mathbf{SD}' \right\|} \tag{25}$$

where $\mathbf{z}$ = vector of the random variables, $\mathbf{z} = \Theta(\mathbf{x}, \quad)$, $\mathbf{J}_{\mathbf{u}^*,\mathbf{z}^*}$ = Jacobian of the probability transformation from the original space $\mathbf{u}$ with respect to the coordinates of the design point $\mathbf{z}^*$ (the most likely failure point), and $\mathbf{SD}'$ = standard deviation matrix of equivalent normal variables $\mathbf{z}'$ defined by the linearized inverse transformation

$\mathbf{z}' = \mathbf{z}^* + \mathbf{J}_{\mathbf{z}^*,\mathbf{u}^*}(\mathbf{u} - \mathbf{u}^*)$ at the design point. The elements of $\mathbf{SD}'$ are the square roots of the corresponding diagonal elements of the covariance matrix $\mathbf{\Sigma}' = \mathbf{J}_{\mathbf{z}^*,\mathbf{u}^*}\mathbf{J}^{\mathbf{T}}{}_{\mathbf{z}^*,\mathbf{u}^*}$ of the variable $\mathbf{z}'$. Figs. 37 through 39 present the importance analysis of each bar diameter over time.

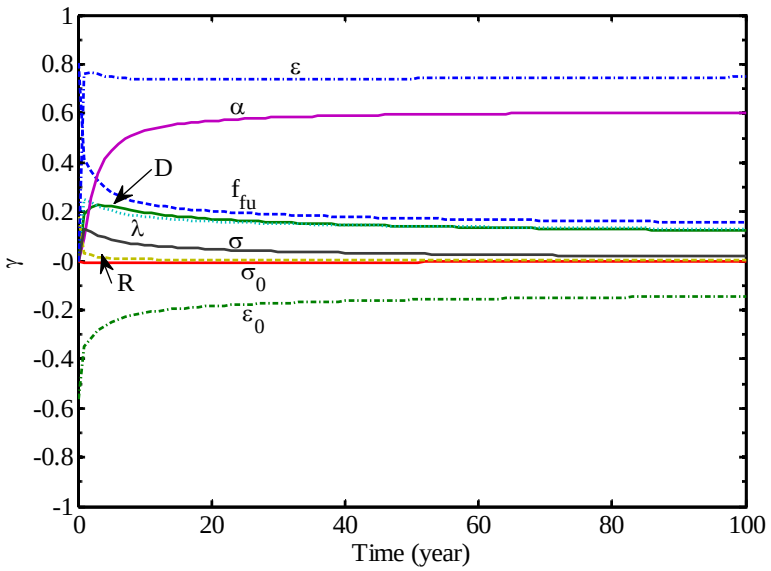

Fig. 37. Importance analysis of 9 mm (0.35 inch) GFRP bars

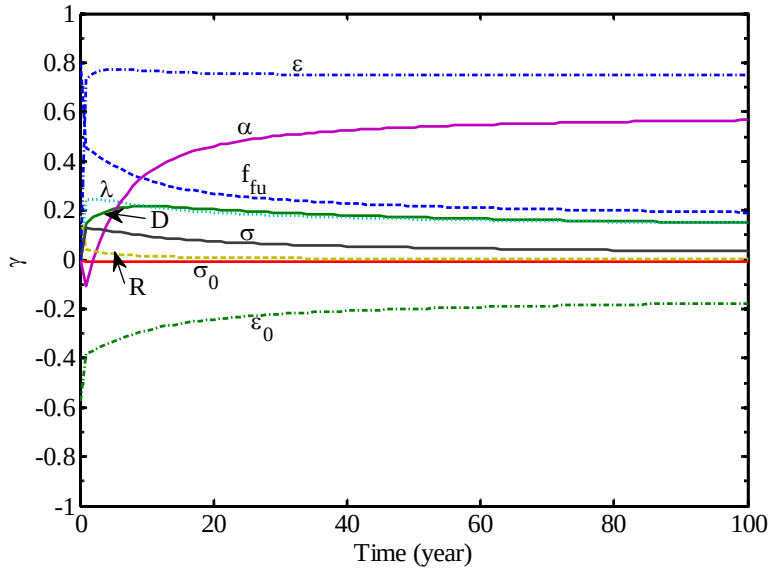

Fig. 38. Importance analysis of 16 mm (0.63 inch) GFRP bars

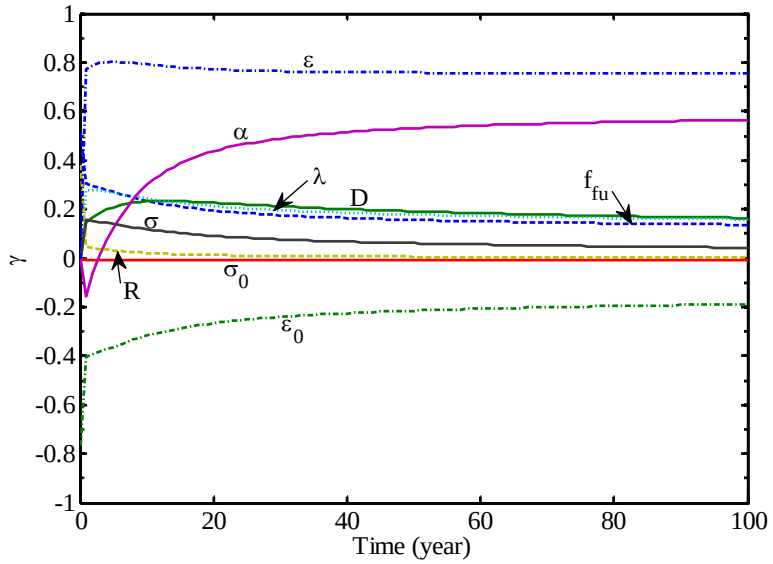

Fig. 39. Importance analysis of 19 mm (0.75 inch) GFRP bars

5.6. Probability of Not Meeting ACI 440 and AASHTO Design Code Over Time

A probabilistic capacity model for predicting the longer-term performance of GFRP bars was used to assess the probability of not meeting ACI 440 and AASHTO design specifications for structures containing GFRP bars. For each bar diameter (#3, #5, and #6), the probability of being below ACI and AASHTO design strength was estimated with the first order reliability method (FORM), and Monte Carlo simulation by using the software FERUM, Mat lab based program for the application of reliability method. Using limit state function described in Equation (21), the probability of not meeting ACI requirement can be expressed as:

$$F_{g_t}(\mathbf{x}) \Theta P\left[g_t(\mathbf{x}, \quad) \le 0\right] \tag{26}$$

In terms of importance analysis, it was inferred that ε_0 and ε are the most important random variables to develop approximate form. Approximate form estimate is obtained by ignoring the uncertainties in model parameters. A point estimates can be obtained using point estimates, $\hat{\mathbf{x}}$, $\hat{\Theta}$ instead of $\mathbf{x}$ and Θ as follows:

$$\begin{aligned} C_t\left(\hat{\mathbf{x}}, \hat{\Theta}\right) &= \hat{\mu}_{C_t} + \hat{\sigma}_{C_t}\varepsilon \\ g_t\left(\hat{\mathbf{x}}, \hat{\Theta}\right) &= C_t\left(\hat{\mathbf{x}}, \hat{\Theta}\right) - C_{aci}(\hat{\mathbf{x}}) = \left(\hat{\mu}_{C_t} + \hat{\sigma}_{C_t}\varepsilon\right) - C_{aci}(\hat{\mathbf{x}}) \end{aligned} \tag{27}$$

where μ_{C_t}, the mean of $C_t(\hat{\mathbf{x}}, \hat{\Theta})$, since ε has standard normal distribution with zero mean and unit variance, $C_t(\hat{\mathbf{x}}, \hat{\Theta})$ and $g_t(\hat{\mathbf{x}}, \hat{\Theta})$ also has normal distribution. Approximate form of probability of not meeting ACI and AASHTO design strength can be written as:

$$F_{g_t} = P\left[g_t\left(\hat{\mathbf{x}},\hat{\boldsymbol{\Theta}}\right) \le 0 \right] \tag{28}$$

Using ACI 440 design tensile strength, $C_{aci}(\mathbf{x})$, Equation (28) can also be written as the approximate form:

$$= \Phi\left(\frac{\hat{\mu}_{C_{aci}} - \hat{\mu}_{C_t}}{\sqrt{\hat{\sigma}_{C_t}^2}} \right) = \Phi\left(\frac{\dfrac{\hat{f}_{fu}}{\mu_{\sigma_0}} - \left[1 - \hat{\lambda}\left(\dfrac{\hat{D}\cdot t}{\hat{R}_0^2} \right)^{\hat{\alpha}} \right]}{\sqrt{\hat{s}_0^{\,2} + \hat{\lambda}^2 \left(\dfrac{\hat{D}\cdot t}{\hat{R}_0^2} \right)^{2\hat{\alpha}} \hat{s}^2}} \right) \tag{29}$$

The reliability index (Ditlevsen and Madsen 1996) corresponding to the probability in Equation (29) was obtained as:

$$\beta = \Phi^{-1}\left\{ 1 - P\left[g_t\left(\hat{\mathbf{x}},\hat{\boldsymbol{\Theta}}\right) \le 0 \right] \right\} \tag{30}$$

where $\Phi^{-1}(\cdot)$ denotes the inverse of the standard normal cumulative distribution function. Under the assumption that limit state function is normal distribution, the first order approximation form can be obtained as:

$$p\left[g_t\left(\mathbf{x},\boldsymbol{\Theta}\right) \le 0 \right] \cong \Phi\left(\frac{\mu_{C_{aci}} - \mu_{C_t}}{\sqrt{\sigma_{C_t}^2 + \sigma_{C_{aci}}^2}} \right) \tag{30}$$

where $\Phi(\cdot)$ denotes the standard normal cumulative distribution function. In the first order approximation, $\mathbf{x}$ and $\boldsymbol{\Theta}$ are random variables and mean and standard deviations of limit state function can be obtained using the first order approximation in Taylor series expansion.

Figs. 40 and 41 represent the probability of not meeting ACI requirement for 9 mm (0.35 inch or, named #3 bars) diameter bar and the first order approximation of each diameter GFRP reinforcements, respectively. The first order approximation form and FORM analysis show relatively accurate values, because they are mostly close to the results of Monte Carlo Simulation. In Fig 41, dotted line, dashed line, and solid line show the probability of #3, #5, and #6, respectively. The probabilistic model indicates that the probability of not meeting ACI 440 and AASHTO design strength after 100 years reaches 0.4, 0.25 and 0.2 for #3, #5 and #6 bars (9, 16, and 19 mm [0.35, 0.63, and 0.75 inch]), respectively. It can be seen that $P[g_t(\mathbf{x},\boldsymbol{\Theta}) \le 0]$ decreases as bar diameter, $\hat{R}_0$, increases as time-dependent. Especially, in the case of smaller bars, ACI and AASHTO design tensile strength is not safe, and the anticipated service-lives of reinforced structures containing smaller GFRP bars may not guaranteed. In the mean while, the GFRP bar with larger diameter exhibits lower degradation rate than smaller bars. It is recommended that ACI and AASHTO design tensile strength is to be changed for smaller diameter GFRP reinforcing bars.

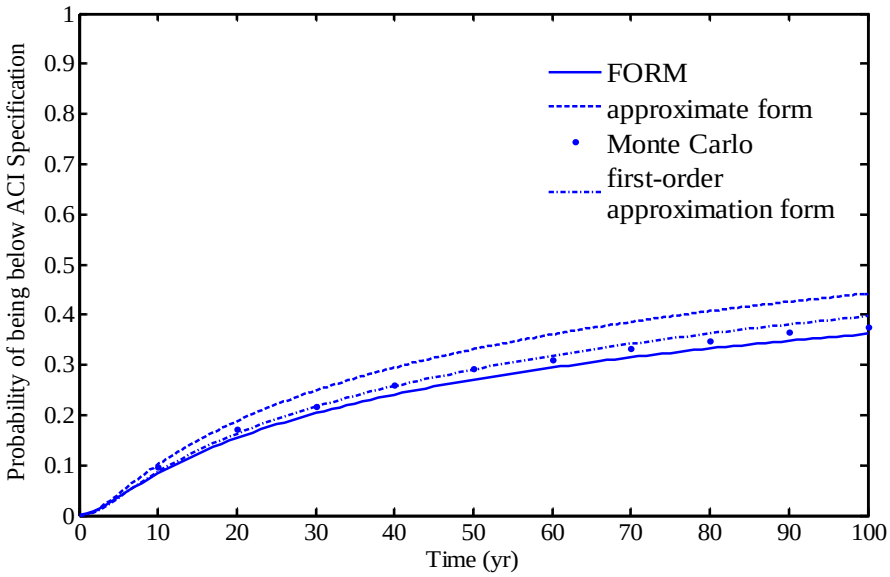

Fig. 40. Probability of not meeting ACI and AASHTO design strength (9 mm [0.35 inch])

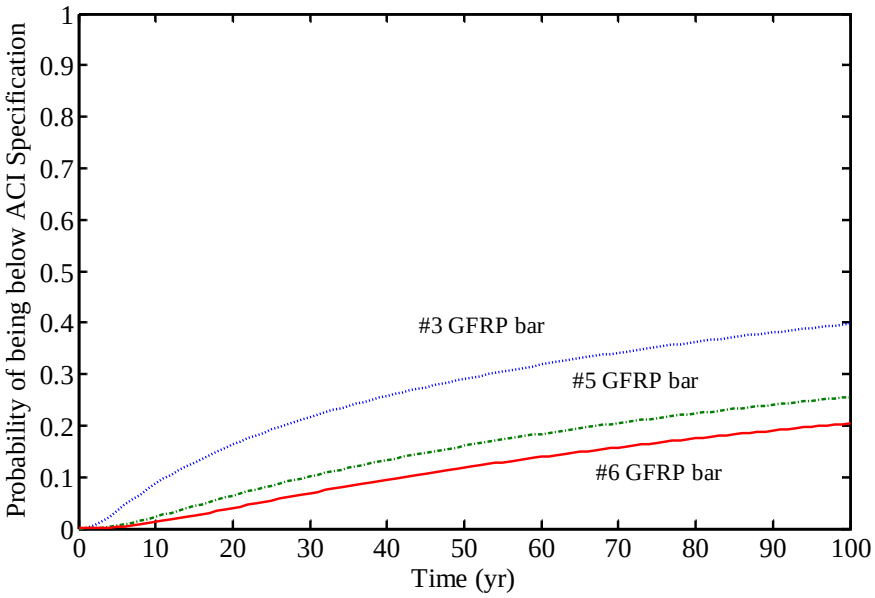

Fig. 41. The first order approximation (9, 16, and 19 mm [0.35, 0.63, and 0.75 inch])

6. CONCLUSIONS

Based on the results of this experimental and analytical investigation, the following conclusions are drawn:

1. The modulus of elasticity of GFRP reinforcement embedded in concrete did not significantly change; however, the tensile strength of extracted GFRP reinforcement from concrete was reduced as a function of time. GFRP reinforcing bars with smaller diameters exhibited faster reductions in tensile strength than the larger diameter bars. In the case of the V1 type bars, the failure initially occurs at wrapping area of the surface of the bars. This failure mode showed that the wrapping could not protect the fibers from the alkali attack.

2. There is insufficient data to determine if the residual tensile strength of the GFRP reinforcing bars is influenced by the pH value of the concrete pore solution, the porosity of concrete, cover depth in concrete, or exposure conditions. Instead, in this research the time dependent reduction of tensile strength was determined to be a function of bar diameter and the diffusion characteristics of the resin matrix.

3. Deterioration was not clearly detected with SEM test; however, the EDX test showed changes in weight percent of chemical elements between exposed and control GFRP reinforcement. FTIR tests showed that there are some changes in amount of the hydroxyl group of C-H and OH ions. However, there is almost no difference in glass transition temperature between control and exposed bars in DSC tests.

4. Based on an existing diffusion model, the predictive capacity model for the longer-term performance of GFRP reinforcing bar was developed using Bayesian updating. The developed probabilistic model is unbiased and properly accounts for the statistical uncertainties in the estimation of unknown parameters and model error associated to the inexact model form. The model shows that the deterioration of bars is fast in the first few years and gradually slows as time increases. The model also predicts that the smaller bars showed faster deterioration rates than larger bars. However, it should be noted that experimental data of #3 diameter GFRP bars used in constructing this prediction modeling were obtained from concrete specimens that were fully saturated, while concrete specimens containing #5 and #6 GFRP bars were exposed to outdoor and were not continuously saturated. If concrete beams containing #5 and #6 bars were saturated or immersed in solution or water, the developed probabilistic model would likely exhibit higher reductions in tensile capacity for GFRP bars as a function of time.

5. The developed probabilistic model was also used to assess the probability of not meeting ACI 440 and AASHTO design strengths over time. For each bar diameter of #3, #5, and #6 of the probability of being below ACI 440 and AASHTO design specifications after 100 years, first order approximation form shows accurate values and the values were calculated as 0.4, 0.25, and 0.2, respectively. It can be seen that $P[g_t(\mathbf{x},\boldsymbol{\Theta}) \le 0]$ decreases as bar diameter, $\hat{R}_0$, increases. In the case of smaller diameter bars (#3), the design tensile strength of ACI 440 and AASHTO design specifications is likely not safe when compared with larger diameter bars.

7. FURTHER RESEARCH

This study indicates that the reduction in tensile capacity of GFRP reinforcing bars in concrete is a function of the diffusion rate of the resin, the bar diameter, and time. In particular, results indicate that the ACI and AASHTO design requirement is not conservative and the structures reinforced with smaller GFRP bars may not reach the anticipated service life of structures. However, further research is required to investigate the effect of GFRP reinforcement deterioration on the performance of GFRP reinforced structures over longer-terms. In addition, further studies on the performance of GFRP reinforced concrete systems in actual environments under sustained or fatigue loadings are recommended.

REFERENCES

Abbasi, A., and Hogg, P. J. (2005). "Temperature and environmental effects on glass fibre rebar: modulus, strength and interfacial bond strength with concrete." *Composites Part B-Engineering*, 36(5), 394-404.

Almusallam T. H., and Al-Salloum Y. A. (2006). "Durability of GFRP rebars in concrete beams under sustained loads at severe environments." *Journal of Composite Materials*, 40(7), 623-637.

American Association of State Highway and Transportation Officials Load and Resistance Factor Design (AASHTO LRFD). (2008) “Bridge design guide specifications for GFRP reinforced concrete decks and traffic railings.” American Association of State Highway and Transportation Officials, Washington, D. C.

American Concrete Institute (ACI). (2007). “Report on fiber-reinforced polymer(FRP) reinforcement for concrete structures.” *ACI 440*, Farmington Hills, MI.

American Concrete Institute (ACI). (2004). “Guide test methods for fiber-reinforced polymers (FRPs) for reinforcing or strengthening concrete structures.” *ACI 440.3R-04*, Farmington Hills, MI.

Antoon, M. K., and Koenig, J. L. (1980). "The structure and moisture stability of the matrix phase in glass-reinforced epoxy composites." *Journal of Macromolecular, Science-Review Macromolecular Chemistry*, C19(1), 135-173.

ASTM. (1997). “Standard test method for density, absorption, and voids in hardened concrete.” *C 642*, West Conshohocken, PA.

ASTM. (2008). “Standard test method for ignition loss of cured reinforced resins.” *D 2584*, West Conshohocken, PA.

Bakis, C.E., Boothby, T.E., Schaut, R.A., and Pantano, C.G. (2005). "Tensile strength of GFRP bars under sustained loading in concrete beams." *Proc., 7th Int. Symposium. Fiber Reinforced Polymer Reinforcement for Concrete Structures, FRPRCS-7*, American Concrete Institute, Farmington Hills, MI, 1429-1446.

Bank, L. C., Gentry, T. R., Thompson, B. P., and Russell, J. S. (2003). "A model specification for FRP composites for civil engineering structures." *Construction and Building Materials*, 17(6-7), 405-437.

Benmokrane, B., Wang, P., Ton-That, T. M., Rahman, H., and Robert, J. F. (2002). "Durability of glass fiber-reinforced polymer reinforcing bars in concrete environment." *Journal of Composites for Construction*, 6(3), 143-153.

Box, G. E. P., and Tiao, G. C. (1992). "*Bayesian inference in statistical analysis*." Addison-Wesley, Reading, MA.

Ceroni, F., Cosenza, E., Gaetano, M., and Pecce, M. (2006). "Durability issues of FRP rebars in reinforced concrete members." *Cement & Concrete Composites*, 28(10), 857-868.

Chen, Y., Davalos, J. F., Ray, I., and Kim, H. Y. (2005). "Accelerated aging tests for evaluations of durability performance of FRP reinforcing bars for concrete structures." *Composite Structures*, 78(1), 101-111.

Chu, W., Wu, L. X., and Karbhari, V. M. (2004). "Durability evaluation of moderate temperature cured E-glass/vinylester systems." *Composite Structures*, 66(1-4), 367-376.

Debaiky, A. S., Nkurunziza, G., Benmokrane, B., and Cousin, P. (2006). "Residual tensile properties of GFRP reinforcing bars after loading in severe environments." *Journal of Composites for Construction*, 10(5), 370-380.

Dejke, V. (2001). "Durability of FRP reinforcement in concrete." M.S. Thesis, Chalmers University of Technology, Götemborg, Sweden.

Der Kiureghian A., and Ke, J. B. (1985). "Finite element based reliability analysis of frame structures." *Proc., 4TH Int. Conference on Structural Safely and Reliability*, Kobe, Japan, 395-404.

Ditlevsen, O., and Madsen, H. O. (1996). *Structural Reliability Methods.* Wiley, New York.

Gardoni, P., Kiureghian, A. D., and Mosalam, K. M. (2002). "Probabilistic capacity models and fragility estimates for reinforced concrete columns based on experimental observations." *Journal of Engineering Mechanics*, 128(10), 1024-1038.

Grasley, Z.C., Lange, D. A., and D' Ambroisa, M.D. (2003). "Internal relative humidity and drying stress gradients in concrete." *Engineering Conferences International, Advances in Cement and Concrete IX*, Copper Mountain, CO, 349-363

Giernacky, R. G., Bakis, C. E., Mostoller, J. D., Boothby, T. E., and Mukherjee, A. (2002). "Evaluation of concrete beams reinforced with internal GFRP bars: A

long-term durability study." *Proc., 2nd Int. Conference on Durability of Fiber Reinforced Polymer (FRP) Composites for Construction (CDCC02),* Montreal, Quebec, Canada, 39-45.

Hohenbichler, M., and Rackwitz, R. (1983). "1st-order concepts in system reliability." *Structural Safety,* 1(3), 177-188.

Iskander, M., and Hassan, M. (2001). "Accelerated degradation of recycled plastic piling in aggressive soils." *Journal of Composite for Construction,* 5(3), 179-187.

Karbhari, V. M., Chin, J. W., Hunston, D., Benmokrane, B., Juska, T., Morgan, R., Lesko, J. J., Sorathia, U., and Reynaud, D. (2003). "Durability gap analysis for fiber-reinforced polymer composites in civil infrastructure." *Journal of Composites for Construction,* 7(3), 238-247.

Katsuki, F., and Uomoto, T. (1995). "Prediction of deterioration of FRP rods due to alkali attack." *Proc., 2nd Int. Symposium (FRPRCS-2), Non-Metallic (FRP) Reinforcement for Concrete Structures,* London, Great Britain, 82-89.

Kim, H. Y., Park, Y. H., You, Y. J., and Moon, C. K. (2007). "Short-term durability tests for GFRP rods under various environmental conditions." *Journal of Composite Structures,* 83(1), 37-47.

Kulkarni, S. (2006). "Calibration of flexural design of concrete members reinforced with FRP bars." M.S. Thesis, Louisiana State University, Baton Rouge, LA.

Litherland, K. L., Oakley, D. R., and Proctor, B. A. (1981). "The use of accelerated ageing procedures to predict the long-term strength of GRC composites." *Cement and Concrete Research,* 11, 455-466.

Micelli, F., and Nanni, A. (2004). "Durability of FRP rods for concrete structures." *Construction and Building Materials*, 18(7), 491-503.

Mufti, A., Banthia, N., Benmokrane, B., Boulfiza, M., and Newhook, J. (2007). "Durability of GFRP composite rods." *Concrete International, American Concrete Institute Magazine*, 29, 37-42.

Mukherjee, A., and Arwikar, S. J. (2005). "Performance of glass fiber-reinforced polymer reinforcing bars in tropical environments - Part I: Structural scale tests." *ACI Structural Journal*, 102(5), 745-753.

Nishizaki, I., and Meiarashi, S. (2002). "Long-term deterioration of GFRP in water and moist environment." *Journal of Composites for Construction*, 6(1), 21-27.

Nkurunziza, G., Benmokrane, B., Debaiky, A. S., and Masmoudi, R. (2005a). "Effect of sustained load and environment on long-term tensile properties of glass fiber-reinforced polymer reinforcing bars." *ACI Structural Journal*, 102(4), 615-621.

Nkurunziza, G., Debaiky, A., Cousin, P., and Benmokrane, B. (2005b). "Durability of GFRP bars: A critical review of the literature." *Progress in Structural Engineering and Materials*, 7(4), 194-209.

Robert, M., Cousin, P., and Benmokrane, B. (2009). "Durability of GFRP reinforcing bars embedded in moist concrete." *Journal of Composites for Construction*, 13(2), 66-73.

Scheirs, J. (2000). *Compositional and failure analysis of polymers*. John Wiley & Sons.

Sen, R., Mullins, G., and Salem, T. (2002). "Durability of E-glass/vinylester reinforcement in alkaline solution." *ACI Structural Journal*, 99(3), 369-375.

Schaefer, B. (2002). "Thermal and environmental effects on fiber reinforced polymer reinforcing bars and reinforced concrete." M.S. Thesis, Texas A&M University, College Station, TX.

Shen, C. H., and Springer, G. S. (1976). "Moisture absorption and desorption of composite materials." *Journal of Composite Materials*, 10, 2-20.

Tannous, F. E., and Saadatmanesh, H. (1998). "Environmental effects on the mechanical properties of E-Glass FRP rebars." *ACI Materials Journal*, 95(2), 87-100.

Tannous, F. E., and Saadatmanesh, H. (1999). "Durability of AR glass fiber reinforced plastic bars." *Journal of Composites for Construction*, 3(1), 12-19.

Trejo, D., Aguiniga, F., Yuan, R., James, R. W., and Keating, P. B. (2005). "Characterization of design parameters for fiber reinforced polymer composite reinforced concrete systems." Texas Transportation Institute Research Report 9-1520-3.

Uomoto, T. (2001). "Durability of FRP reinforcement as concrete reinforcement." *FRP Composites in Civil Engineering*, 1, 85-96.

Vijay, P.V., and Gangarao, H.V.S. (1999). "Accelerated natural weathering of glass fibre reinforced plastic bars." *Proc., 4th International Conference on Fibre Reinforced Plastics for Reinforced Concrete Structures*, Baltimore, MD, I-4, 605-614.

APPENDIX A

The measured data for the control and the extracted GFRP bars of 16 and 19 mm (0.63 and 0.75 inch, referred #5 and #6, respectively) was tabulated in Table A.1. Normalized tensile capacity of each bar type and each bar diameter ($\sigma_t / \mu_{\sigma_0}$) was provided in Table A.2. To calculate the normalized data for each bar type and each bar diameter, the residual tensile capacity data (after 7 years exposure) was divided by the measured mean value of tensile capacity data of each bar type and each bar diameter GFRP bars before exposure (at time 0). The normalized tensile capacity data was used as experimental observations when Bayesian updating was performed to estimate the set of unknown parameters in an updated probabilistic model.

Table A.1. Tensile test results for the control and extracted GFRP bars

Results from Tension Tests (ksi)												
Bar Diameter	#5 (16 mm, 0.63 inch)						#6 (19 mm, 0.75 inch)					
Time (years)	0			7 (σ_t)			0			7 (σ_t)		
Specimen #	V1	V2	P	V1	V2	P	V1	V2	P	V1	V2	P
1	76.39	76.67	98.93	70.31	58.06	96.71	83.28	75.87	103.47	69.19	56.53	93.00
2	93.26	77.10	95.42	76.87	56.42	92.25	73.79	72.29	97.34	63.18	58.71	92.60
3	96.78	75.10	101.32	69.35	60.25	90.48	73.32	73.70	97.59	68.13	55.90	82.81
4	90.77	71.67	103.81	92.23	57.85	82.65	83.18	73.00	93.82	52.89	57.38	82.23
5	85.34	71.82	99.98	51.90	56.65	90.41	77.17	70.22	94.41	56.44	52.45	92.75
6			103.84	74.45	54.85	88.34	82.95	73.94	101.12	68.28	58.26	94.78
7			101.98	49.51	50.04	89.16	72.31	72.72	96.31	56.44	57.34	93.22
8			97.66	70.79	52.83	85.52	73.32	73.32	99.94	56.30	57.23	90.41
9			101.42	72.89	55.31	86.72	79.03	71.97	100.29	54.91	60.67	93.60
10			97.26	84.97	52.94	83.50	75.44	71.46	96.02	65.03	52.90	96.48
11				84.51	56.55	73.91				71.29	55.89	85.82
12				88.98	56.62	90.01				63.67	53.30	86.06
13				69.15	53.80	89.28				64.00	59.37	87.52
14				74.24	54.93	89.40				65.48	57.47	93.78
15				65.91	49.82	81.78				67.93	56.58	86.71
16				66.32	54.73					67.65	61.80	94.04
17				72.32	56.39					58.50	64.80	96.62
18				67.06	54.46					56.80		96.97
19				93.59	54.78					61.10		92.61
20				94.65	55.95					50.24		94.68
21				77.90	52.87					51.19		87.95
22				89.55	56.76					69.16		91.34
23				92.88	53.32					55.91		87.46
24				88.88	53.03					58.98		92.39
25				88.40	51.97					67.83		88.08
26				69.80	55.90					56.19		88.59
27				84.95	56.34					58.61		92.08
28				84.11	54.18					58.99		89.88
29				83.86	55.38					62.57		90.17
30				80.54	56.95							89.80
31				83.75								91.09
32				79.92								93.68
33				72.01								
34				82.55								
35				77.96								
Average (μ_{σ_0})	88.51	74.47	100.16	77.92	55.00	87.34	77.38	72.85	98.03	61.27	57.45	90.91
st.dev.	7.95	2.60	2.83	10.91	2.28	5.36	4.44	1.54	3.10	5.99	3.15	3.77

Table A.2. Normalized tensile test results for the control and extracted GFRP bars

Normalized Tensile Capacity = $(\sigma_t / \mu_{\sigma_0})$												
Bar Diameter	#5 (16 mm, 0.63 inch)						#6 (19 mm, 0.75 inch)					
Time (years)	0			7 (σ_t)			0			7 (σ_t)		
Test #	V1	V2	P	V1	V2	P	V1	V2	P	V1	V2	P
1	0.86	1.03	0.99	0.79	0.78	0.97	1.08	1.04	1.06	0.89	0.78	0.95
2	1.05	1.04	0.95	0.87	0.76	0.92	0.95	0.99	0.99	0.82	0.81	0.94
3	1.09	1.01	1.01	0.78	0.81	0.90	0.95	1.01	1.00	0.88	0.77	0.84
4	1.03	0.96	1.04	1.04	0.78	0.83	1.07	1.00	0.96	0.68	0.79	0.84
5	0.96	0.96	1.00	0.59	0.76	0.90	1.00	0.96	0.96	0.73	0.72	0.95
6			1.04	0.84	0.74	0.88	1.07	1.01	1.03	0.88	0.80	0.97
7			1.02	0.56	0.67	0.89	0.93	1.00	0.98	0.73	0.79	0.95
8			0.98	0.80	0.71	0.85	0.95	1.01	1.02	0.73	0.79	0.92
9			1.01	0.82	0.74	0.87	1.02	0.99	1.02	0.71	0.83	0.95
10			0.97	0.96	0.71	0.83	0.97	0.98	0.98	0.84	0.73	0.98
11				0.95	0.76	0.74				0.92	0.77	0.88
12				1.01	0.76	0.90				0.82	0.73	0.88
13				0.78	0.72	0.89				0.83	0.81	0.89
14				0.84	0.74	0.89				0.85	0.79	0.96
15				0.74	0.67	0.82				0.88	0.78	0.88
16				0.75	0.73					0.87	0.85	0.96
17				0.82	0.76					0.76	0.89	0.99
18				0.76	0.73					0.73		0.99
19				1.06	0.74					0.79		0.94
20				1.07	0.75					0.65		0.97
21				0.88	0.71					0.66		0.90
22				1.01	0.76					0.89		0.93
23				1.05	0.72					0.72		0.89
24				1.00	0.71					0.76		0.94
25				1.00	0.70					0.88		0.90
26				0.79	0.75					0.73		0.90
27				0.96	0.76					0.76		0.94
28				0.95	0.73					0.76		0.92
29				0.95	0.74					0.81		0.92
30				0.91	0.76							0.92
31				0.95								0.93
32				0.90								0.96
33				0.81								
34				0.93								
35				0.88								
Average (μ_{σ_0})	1	1	1	0.88	0.74	0.87	1	1	1	0.79	0.79	0.93
st.dev.	0.09	0.03	0.03	0.12	0.03	0.05	0.06	0.02	0.03	0.08	0.04	0.04

APPENDIX B

The MOE test results for the control and exposed bars from MOE testing were tabulated in Table B.1 through B.3. Based on the test results, the statistical t-tests of equality at a 0.05 level of significance were performed to determine if the mean MOE of exposed GFRP bars differs from the mean MOE of the control bars. The MOE of exposed bars as a function of actual cover depth were compared to the MOE of control bars. The measured MOE values of control bars were obtained from preliminary tension tests with two loading type A and B. As previously mentioned in preliminary tension tests, the one set of control GFRP bars were preloaded, unloaded, and reloaded to failure as loading type A, and other set were loaded directly to failure as loading type B. Based on the statistical t-tests results, it was concluded that there is no statistical evidence that the mean MOE of GFRP bars between loading type A and B are different. The preliminary test results obtained from loading type A and B were used as control MOE values to estimate the changes in MOE of exposed GFRP bars in the statistical t-tests.

Table B.1. MOE test results for bar type V1

V1 #5 (16 mm, 0.63 inch)		V1 #6 (19 mm, 0.75 inch)	
MOE - No exposure ksi (Mpa)	MOE - After Exposure ksi (Mpa)	MOE - No exposure ksi (Mpa)	MOE - After Exposure ksi (Mpa)
6952 (47932)	5617 (38726)	6304 (43466)	4290 (29577)
5921 (40824)	5689 (39222)	6414 (44221)	5915 (40783)
6452 (44485)	5489 (37843)	6525 (44991)	5866 (40442)
5866 (40445)	5759 (39705)	6940 (47848)	5820 (40124)
6204 (42775)	2151 (14829)	6256 (43131)	6746 (46512)
	5823 (40149)	6032 (41587)	6012 (41451)
	5271 (36340)	6441 (44412)	5990 (41302)
	5327 (36726)	6557 (45211)	5393 (37181)
	5696 (39272)	6265 (43193)	6450 (44474)
	5505 (37956)		6277 (43276)
	5397 (37213)		6461 (44584)
	5855 (40370)		5840 (40268)
	6133 (42283)		6419 (44254)
	5978 (41215)		6207 (42795)
	5830 (40199)		6116 (42169)
	5894 (40640)		6666 (45962)
	5346 (36857)		5536 (38167)
	5319 (36674)		5975 (41193)
	5913 (40771)		5945 (40988)
	5415 (37332)		5964 (41120)
	5718 (39422)		5838 (40252)
	5092 (35108)		6026 (41547)
	5829 (40193)		5830 (40195)
	5698 (39288)		6379 (43985)
	5728 (39491)		6280 (43296)
	4325 (29822)		5470 (37713)
	6056 (41755)		6684 (46083)
	5780 (39854)		5134 (35399)
	5919 (40812)		6439 (44396)
	5860 (40401)		
	5487 (37830)		
	6026 (41550)		
	5605 (38646)		
Mean	**Mean**	**Mean**	**Mean**
Standard Deviation	**Standard Deviation**	**Standard Deviation**	**Standard Deviation**
6279 (43292)	5531 (38136)	6415 (44229)	5999 (41360)
444 (3061)	697 (4809)	254 (1751)	510 (3518)

Table B.2. MOE test results for bar type V2

V2 #5 (16 mm, 0.63 inch)		V2 #6 (19 mm, 0.75 inch)	
MOE - No exposure ksi (Mpa)	MOE - After Exposure ksi (Mpa)	MOE - No exposure ksi (Mpa)	MOE - After Exposure ksi (Mpa)
6912 (47657)	5394 (37188)	5810 (40059)	5866 (40443)
6878 (47077)	5394 (37191)	5724 (39463)	5764 (39740)
6320 (43575)	5382 (37106)	5827 (40174)	3814 (26299)
6103 (42079)	5376 (37066)	5850 (40333)	5622 (38759)
5656 (38997)	5604 (38639)	5674 (39124)	5779 (39845)
	5040 (34748)	5511 (38000)	5977 (41212)
	5309 (36602)	5609 (38674)	5909 (40743)
	5947 (41001)	5743 (39594)	5605 (38642)
	5607 (38656)	5730 (39509)	5940 (40953)
	5511 (37995)	5532 (38142)	5542 (38210)
	5628 (38802)		5752 (39658)
	5564 (38361)		6087 (41969)
	5419 (37361)		5901 (40685)
	5602 (38628)		5749 (39641)
	5103 (35186)		5837 (40244)
	5679 (39157)		
	5634 (38845)		
	5964 (41122)		
	5310 (36609)		
	5495 (37887)		
	5418 (37359)		
	5605 (38644)		
	5953 (41041)		
	5496 (37893)		
	5316 (36653)		
	5276 (36377)		
	3540 (24407)		
	5551 (38273)		
	5626 (38793)		
Mean	**Mean**	**Mean**	**Mean**
Standard Deviation	**Standard Deviation**	**Standard Deviation**	**Standard Deviation**
6374 (43947)	5439 (37503)	5701 (39307)	5719 (39432)
533 (3675)	426 (2937)	119 (818)	516 (3555)

Table B.3. MOE test results for bar type P

P #5 (16 mm, 0.63 inch)		P #6 (19 mm, 0.75 inch)	
MOE - No exposure ksi (Mpa)	MOE - After Exposure ksi (Mpa)	MOE - No exposure ksi (Mpa)	MOE - After Exposure ksi (Mpa)
6237 (43003)	3501 (24138)	5893 (40628)	4666 (32172)
4854 (33467)	5051 (34823)	5686 (39202)	5580 (38474)
5846 (40307)	5336 (36788)	6086 (41960)	5416 (37344)
5197 (35832)	5591 (38549)	6525 (44991)	5955 (41056)
	5654 (38982)	6940 (47848)	5709 (39365)
	5379 (37089)	5657 (39005)	5337 (36795)
	6547 (45139)	5750 (39646)	5601 (38619)
	5693 (39253)	5852 (40347)	5572 (38415)
	5671 (39101)	6557 (45211)	5662 (39041)
	5498 (37906)	6265 (43193)	5427 (37416)
	5861 (40412)		5574 (38428)
	5323 (36699)		5820 (40126)
	5757 (39694)		5892 (40622)
	5404 (37261)		5492 (37866)
	5789 (39912)		5885 (40576)
			5666 (39066)
			5417 (37348)
			5444 (37535)
			5400 (37233)
			5454 (37603)
			5515 (38025)
			5316 (36653)
			5737 (39558)
			5807 (40040)
			5651 (38961)
			5757 (39696)
			5553 (38290)
			5596 (38584)
			5913 (40767)
			5607 (38659)
			5819 (40122)
			5760 (39711)
Mean	**Mean**	**Mean**	**Mean**
Standard Deviation	**Standard Deviation**	**Standard Deviation**	**Standard Deviation**
5534 (38156)	5470 (37716)	6121 (42203)	5594 (38568)
624 (4302)	640 (4415)	436 (3008)	244 (1683)

Table B.4. The t-test results for MOE of V1 #5 GFRP bars

BAR	V1 #5					
	#5(1.25-2.25 inch)		#5(2.25-2.5 inch)		#5(2.5-3.5 inch)	
	Beam 20/1.25"	A+B	Beam 5/2.25"	A+B	Beam 8/2.5"	A+B
	Beam 19/1.25"		Beam 31/2.25"		Beam 29/3.5"	
	Beam 5/2.25"		Beam 8/2.5"			
	Beam 31/2.25"					
1	5616.67	5840.88	5695.93	5840.88	5829.48	5840.88
2	5688.72	5736.80	5505.01	5736.80	5698.19	5736.80
3	5488.62	5789.00	5397.25	5789.00	5727.73	5789.00
4	5758.70	5738.12	5855.19	5738.12	4325.29	5738.12
5	2150.77	5807.65	6132.69	5807.65	6056.01	5807.65
6	5823.07	5384.50	5977.75	5384.50	5780.36	5384.50
7	5270.64	5827.72	5830.41	5827.72	5919.23	5827.72
8	5326.62	5806.35	5894.28	5806.35	5859.67	5806.35
9	5695.93	5807.60	5345.61	5807.60	5486.71	5807.60
10	5505.01	5637.36	5319.06	5637.36	6026.31	5637.36
11	5397.25		5913.39		5605.20	
12	5855.19		5414.58			
13	6132.69		5717.65			
14	5977.75		5091.94			
15	5830.41		5829.48			
16	5894.28		5698.19			
17	5345.61		5727.73			
18	5319.06		4325.29			
19	5913.39		6056.01			
20	5414.58		5780.36			
21	5717.65					
22	5091.94					
Average	5464.30	5737.60	5625.39	5737.60	5664.93	5737.60
Standard Deviation	787.09	137.72	408.46	137.72	475.56	137.72
Coefficients of Variation	0.14	0.02	0.07	0.02	0.08	0.02
n	22	10	20	10	11	10
x(mean)	5464.30	5737.60	5625.39	5737.60	5664.93	5737.60
S	787.09	137.72	408.46	137.72	475.56	137.72
SP^2	439342.41		119306.73		128013.17	
SP	662.83		345.41		357.79	
to	-1.08		-0.84		-0.46	
n1+n2-2	30		28		19	
t0.025, n1+n2-2	2.042		2.048		2.093	
reject or not	not rejected		not rejected		not rejected	
T0*	-1.58		-1.11		-0.48	
ν	24		26		12	
t0.025, ν	2.07		2.06		2.20	
reject or not	not rejected		not rejected		not rejected	

Table B.5. The t-test results for MOE of V1 #6 GFRP bars

BAR	V1 #6									
	#6 (1-1.25 inch)		#6 (1.25-2 inch)		#6 (2-2.25 inch)		#6 (2.25-2.5 inch)		#6 (2.5-3 inch)	
	Beam 15/1" / Beam 21/1.25"	A+B	Beam 21/1.25" / Beam 9/2"	A+B	Beam 9/2" / Beam 4/2.25"	A+B	Beam 4/2.25" / Beam 1/2.5"	A+B	Beam 1/2.5" / Beam 28/3"	A+B
1	4289.85	6255.60	6012.01	6255.60	6276.71	6255.60	6116.05	6255.60	5963.91	6255.60
2	5915.13	6031.66	5990.28	6031.66	6461.15	6031.66	6666.26	6031.66	5838.12	6031.66
3	5865.57	6441.40	5392.63	6441.40	5840.45	6441.40	5535.70	6441.40	6025.85	6441.40
4	5819.50	6557.23	6450.36	6557.23	6418.52	6557.23	5974.52	6557.23	5829.82	6557.23
5	6745.94	6264.67	6276.71	6264.67	6206.84	6264.67	5944.82	6264.67	6379.49	6264.67
6	6012.01	6304.24	6461.15	6304.24	6116.05	6304.24	5963.91	6304.24	6279.60	6304.24
7	5990.28	6413.70	5840.45	6413.70	6666.26	6413.70	5838.12	6413.70	5469.75	6413.70
8	5392.63	6525.39	6418.52	6525.39	5535.70	6525.39	6025.85	6525.39	6683.71	6525.39
9	6450.36	6939.83	6206.84	6939.83	5974.52	6939.83	5829.82	6939.83	5134.17	6939.83
10					5944.82		6379.49		6439.16	
Average	5831.25	6414.86	6116.55	6414.86	6144.10	6414.86	6027.45	6414.86	6004.36	6414.86
Standard Deviation	694.13	253.92	350.42	253.92	333.60	253.92	310.96	253.92	467.89	253.92
Coefficients of Variation	0.12	0.04	0.06	0.04	0.05	0.04	0.05	0.04	0.08	0.04
n	9	9	9	9	10	9	10	9	10	9
x(mean)	5831.25	6414.86	6116.55	6414.86	6144.10	6414.86	6027.45	6414.86	6004.36	6414.86
S	694.13	253.92	350.42	253.92	333.60	253.92	310.96	253.92	467.89	253.92
SP^2	273148.18		93632.90		89258.66		81531.67		146239.63	
SP	522.64		305.99		298.76		285.54		382.41	
to	-2.37		-2.07		-1.97		-2.95		-2.34	
n1+n2-2	16		16		17		17		17	
t0.025, n1+n2-2	2.120		2.120		2.110		2.110		2.110	
reject or not	rejected		not rejected		not rejected		rejected		rejected	
T0*	-2.37		-2.07		-2.00		-2.99		-2.41	
ν	10		15		17		17		14	
t0.025, ν	2.23		2.14		2.12		2.12		2.14	
reject or not	rejected		not rejected		not rejected		rejected		rejected	

Table B.6. The t-test results for MOE of V2 #5 GFRP bars

BAR	V2 #5					
	#5 (1-1.5 inch)		#5 (1.5-2.25 inch)		#5 (2.25-3 inch)	
	Beam 23/1" Beam 14/1.5"	A+B	Beam 14/1.5" Beam 13/2.25" Beam 30/2.25"	A+B	Beam 13/2.25" Beam 30/2.25" Beam 2/3" Beam 32/3"	A+B
1	5393.72	5637.46	5039.75	5637.46	5510.66	5637.46
2	5394.14	5625.96	5308.68	5625.96	5627.79	5625.96
3	5381.73	5635.50	5946.71	5635.50	5563.81	5635.50
4	5375.92	5532.84	5606.58	5532.84	5418.80	5532.84
5	5604.16	5482.28	5510.66	5482.28	5602.45	5482.28
6	5039.75	5558.43	5627.79	5558.43	5103.36	5558.43
7	5308.68	5659.64	5563.81	5659.64	5679.22	5659.64
8	5946.71	5327.22	5418.80	5327.22	5633.96	5327.22
9	5606.58	5546.25	5602.45	5546.25	5964.18	5546.25
10			5103.36		5309.70	
11			5679.22		5495.00	
12			5633.96		5418.45	
13			5964.18		5604.78	
14			5309.70		5952.53	
15					5495.98	
16					5316.11	
17					5276.02	
18					3539.92	
19					5551.02	
20					5626.41	
Average	5450.15	5556.18	5522.55	5556.18	5434.51	5556.18
Standard Deviation	249.93	104.29	270.17	104.29	490.85	104.29
Coefficients of Variation	0.05	0.02	0.05	0.02	0.09	0.02
n	9	9	14	9	20	9
x(mean)	5450.15	5556.18	5522.55	5556.18	5434.51	5556.18
S	249.93	104.29	270.17	104.29	490.85	104.29
SP^2	36670.27		49328.99		172770.82	
SP	191.49		222.10		415.66	
to	-1.17		-0.35		-0.73	
n1+n2-2	16		21		27	
t0.025, n1+n2-2	2.120		2.080		2.052	
reject or not	not rejected		not rejected		not rejected	
T0*	-1.17		-0.42		-1.06	
ν	11		18		22	
t0.025, ν	2.23		2.10		2.07	
reject or not	not rejected		not rejected		not rejected	

Table B.7. The t-test results for MOE of V2 #6 GFRP bars

BAR	V2 #6					
	#6 (1-1.5 inch)		#6 (1.5-2.25 inch)		#6 (2.25-3 inch)	
	Beam 18/1"	A+B	Beam 16/1.25"	A+B	Beam 7/2"	A+B
	Beam 16/1.25"		Beam 7/2"		Beam 36/2"	
			Beam 36/2"		Beam 12/3"	
					Beam 26/3"	
1	5865.81	5511.40	5621.59	5511.40	5977.32	5511.40
2	5763.73	5609.25	6050.58	5609.25	5909.22	5609.25
3	3814.28	5742.67	6031.56	5742.67	5604.56	5742.67
4	5621.59	5730.33	5779.07	5730.33	5939.71	5730.33
5	6050.58	5532.02	5977.32	5532.02	5541.90	5532.02
6	6031.56	5810.13	5909.22	5810.13	5751.97	5810.13
7	5779.07	5723.58	5604.56	5723.58	6087.03	5723.58
8		5826.71	5939.71	5826.71	5900.86	5826.71
9		5849.82	5541.90	5849.82	5749.47	5849.82
10		5674.41		5674.41	5836.87	5674.41
Average	5560.94	5701.03	5828.39	5701.03	5829.89	5701.03
Standard Deviation	785.00	118.60	196.57	118.60	169.16	118.60
Coefficients of Variation	0.14	0.02	0.03	0.02	0.03	0.02
n	7	10	9	10	10	10
x(mean)	5560.94	5701.03	5828.39	5701.03	5829.89	5701.03
S	785.00	118.60	196.57	118.60	169.16	118.60
SP^2	254931.40		25630.98		21341.21	
SP	504.91		160.10		146.09	
to	-0.56		1.73		1.97	
n1+n2-2	15		17		18	
t0.025, n1+n2-2	2.131		2.110		2.101	
reject or not	not rejected		not rejected		not rejected	
T0*	-0.47		1.69		1.97	
ν	6		13		16	
t0.025, ν	2.45		2.18		2.12	
reject or not	not rejected		not rejected		not rejected	

Table B.8. The t-test results for MOE of P #5 GFRP bars

BAR	p #5					
	#5 (1.25-1.5 inch)		#5 (1.5-2.25 inch)		#5 (2.25-3 inch)	
	Beam 22/1.25"	A+B	Beam 25/1.5"	A+B	Beam 3/2.25"	A+B
	Beam 25/1.5"		Beam 3/2.25"		Beam 10/2.25"	
			Beam 10/2.25"		Beam 6/3"	
					Beam 27/3"	
1	3500.89	5647.66	5379.32	5647.66	5379.32	5647.66
2	5050.61	5572.83	6546.79	5572.83	6546.79	5572.83
3	5335.64	5539.47	5693.19	5539.47	5693.19	5539.47
4	5591.08	4670.91	5671.06	4670.91	5671.06	4670.91
5	5653.92	5580.77	5497.83	5580.77	5497.83	5580.77
6		5635.37		5635.37	5861.20	5635.37
7		7364.90		7364.90	5322.72	7364.90
8		5396.92		5396.92	5757.13	5396.92
9		4713.67		4713.67	5404.21	4713.67
10		5639.40		5639.40	5788.80	5639.40
Average	5026.43	5576.19	5757.64	5576.19	5692.23	5576.19
Standard Deviation	885.44	730.99	459.63	730.99	354.02	730.99
Coefficients of Variation	0.18	0.13	0.08	0.13	0.06	0.13
n	5	10	5	10	10	10
x(mean)	5026.43	5576.19	5757.64	5576.19	5692.23	5576.19
S	885.44	730.99	459.63	730.99	354.02	730.99
SP^2	611163.46		434932.60		329838.71	
SP	781.77		659.49		574.32	
to	-1.28		0.50		0.45	
n1+n2-2	13		13		18	
t0.025, n1+n2-2	2.160		2.160		2.101	
reject or not	not rejected		not rejected		not rejected	
T0*	-1.20		0.59		0.45	
ν	7		12		13	
t0.025, ν	2.45		2.20		2.16	
reject or not	not rejected		not rejected		not rejected	

Table B.9. The t-test results for MOE of P #6 GFRP bars

BAR	p #6					
	#6 (1.25-1.5 inch)		#6 (1.5-2.25 inch)		#6 (2.25-3 inch)	
	Beam 24/1.25"	A+B	Beam 17/1.5"	A+B	Beam 11/2.25"	A+B
	Beam 17/1.5"		Beam 11/2.25"		Beam 35/2.25"	
			Beam 35/2.25"		Beam 33/3"	
					Beam 34/3"	
1	4666.17	5657.14	5601.14	5657.14	5819.79	5657.14
2	5580.15	5750.12	5571.56	5750.12	5891.78	5750.12
3	5416.25	5851.85	5662.49	5851.85	5492.02	5851.85
4	5954.70	6557.23	5426.72	6557.23	5885.03	6557.23
5	5709.37	6264.67	5573.55	6264.67	5666.00	6264.67
6	5336.61	5892.61	5819.79	5892.61	5737.41	5892.61
7	5601.14	5685.78	5891.78	5685.78	5807.27	5685.78
8	5571.56	6085.75	5492.02	6085.75	5650.81	6085.75
9	5662.49	6525.39	5885.03	6525.39	5757.43	6525.39
10	5426.72	6939.83	5666.00	6939.83	5553.48	6939.83
11	5573.55		5416.93		5596.13	
12			5443.96		5912.71	
13			5400.16		5607.05	
14			5453.79		5819.24	
15			5515.06		5759.62	
16			5316.04			
Average	5499.88	6121.04	5571.00	6121.04	5730.38	6121.04
Standard Deviation	322.26	436.26	175.06	436.26	130.51	436.26
Coefficients of Variation	0.06	0.07	0.03	0.07	0.02	0.07
n	11	10	16	10	15	10
x(mean)	5499.88	6121.04	5571.00	6121.04	5730.38	6121.04
S	322.26	436.26	175.06	436.26	130.51	436.26
SP^2	144814.21		90526.85		84843.47	
SP	380.54		300.88		291.28	
to	-3.74		-4.53		-3.29	
n1+n2-2	19		24		23	
t0.025, n1+n2-2	2.093		2.064		2.069	
reject or not	rejected		rejected		rejected	
T0*	-3.68		-3.80		-2.75	
ν	16		11		10	
t0.025, ν	2.12		2.23		2.23	
reject or not	rejected		rejected		rejected	

VITA

Name Jeongjoo Kim

Address Zachry Department of Civil Engineering

Texas A&M University

College Station Texas 77843-3136

Email: jeongjookim79@gmail.com

Education B.S. 2005 Kyungwon University, South Korea

M.S. 2010 Texas A&M University, College Station, USA